3D FACIAL MODEL ANALYSIS

FOR CLINICAL MEDICINE

LIU YI LIN

NATIONAL UNIVERSITY OF SINGAPORE

2013

3D FACIAL MODEL ANALYSIS

FOR CLINICAL MEDICINE

LIU YI LIN

(M.Eng. Jilin University, China)

A THESIS SUBMITTED FOR THE DEGREE OF DOCTOR OF PHILOSOPHY

DEPARTMENT OF MECHANICAL ENGINEERING
NATIONAL UNIVERSITY OF SINGAPORE

2013

Declaration

I hereby declare that this thesis is my original work and it has been written by me in its entirety. I have duly acknowledged all the sources of information which have been used in the thesis.

This thesis has also not been submitted for any degree in any university previously.

Liu Yi Lin

Dec 2013

Acknowledgments

First I must express my sincere appreciation to my supervisor, Associate Professor Lee Heow Pueh for his invaluable direction, great patient, continuous support and personal encouragement throughout my PhD studies. I indeed have not only obtained a considerable number of fresh ideas from the discussions with him, but also learned and benefitted from his insightful comments and critiques.

I would like to thank Dr Ngo Yeow Seng Raymond, Associate Professor Kelvin Foong, Dr Lee Shu Jin, Dr Saurabh Garg and Mr Tok Wee Wah who have made my study possible through their generous guidance and support.

I gratefully acknowledge the financial support provided by National University of Singapore through the Research Scholarship without which it would have not been possible for me to have the chance of working for my degree in NUS.

I also want to express my great thanks to all the lab officers and friends in the Dynamic Lab for their support and encouragement in the course of my PhD study. Finally special thanks to my parent for their endless love and support. I would not have been able to finish this thesis without their encouragement.

Liu Yi Lin
Dec 2013

Table of contents

Abstract

This thesis aims to investigate both facial paralysis diagnosis and facial highlight features based on 2D and 3D facial models.

First, a novel automated objective asymmetry grading system is developed for facial paralysis diagnosis. The development of this grading system combines observations and clinical assessments of the patients for different degrees of motion dysfunction in various facial expressions. To improve the performance of the system, higher order surface properties in facial imaging technique for 3D model analysis are used. Also, to overcome the subjectivity of diagnosis encountered by the landmark based computer aided grading methods, facial symmetry grading is carried out based on fine registration result of the original and mirror facial mesh by the iterated closest-point algorithm (ICP), which does not rely on any landmarks. Moreover, to avoid overfitting caused by small sample set, the noise injected artificial neural networks (ANNs) in feature extraction and classification for 3D objects were implemented. Compared with standard ANNs, the accuracy, sensitivity and specificity of the

proposed noise-injected ANNs are significantly improved. The system is also tested with data of patients having follow-up treatment and diagnosis after the initial treatment. The proposed ANN system can detect the improvement of the patients quite well. A plausible explanation of the appreciably improved performance is that the injected noise increases the generalization ability, and reduces the sensitivity to the disturbance in this manner.

Meanwhile, the highlight feature patterns of natural faces are explored as a planning aid for plastic surgery. Different from previous reported studies on attractive face patterns, which have mainly based their criteria on facial profile, this study intends to determine the position and shape of the highlights of natural faces across race and gender. Some relevant conclusions can be drawn from the present study. First, nasal highlights are discontinuous, thus the implant or filler should keep the dorsum and tip at different levels. Second, the shape of the nasion saddle is intimately associated with race. Also, the forehead highlight has mainly two types, T shape and maple leaf shape. The distributions of these two types are closely related to race and gender.

List of Tables

List of Figures

Acronyms

2D	Two-Dimensional
3D	Three-Dimensional
AI	Artificial Intelligence
ANNs	Artificial neural networks
BP	Back-Propagation
CT	Computed Tomography
FP	Facial Paralysis
FPRP	Facial Paralysis Recovery Profile
HBGS	House-Brackmann grading system
HSV-1	Herpes Simplex Virus type 1
ICP	Iterative Closest Point
MLP	Multilayer Perceptrons

MRI	Magnetic Resonance Imaging
RMS	Root mean square
SFGS	Sunnybrook Facial Grading System
VZV	Varicella-zoster virus

Chapter 1. Introduction

The face region would be the primary visual identifier of a human being, and it carries remarkable significance of biological vitality and aesthetic beauty or as a way of communication through various facial expressions. Given the importance of the face, it is no wonder that all through the mankind history, attempts have been made to understand the features of the face. Over the years, scientists have shown a keen interest in facial feature analysis studies. Their studies are not limited to aesthetic research, but involved in facial identification, facial expression recognition, differential analysis of gender, age and race, and other aspects. There are various applications of these studies in a large number of areas, such as face recognition system for identity recognition and security check,[1] automated face age-verification system for cigarette vending machines,[2] and human face and smile detection system for digital camera.[3,4] All these successful applications have proved the advanced character of facial feature analysis technology.

Meanwhile, the great advances in computer image techniques have opened new perspectives for facial feature analysis. Traditional two-

dimensional (2D) image based studies have been extended to three-dimensional (3D) image analysis by high quality 3D image reconstruction technologies such as computed tomography (CT) scan, magnetic resonance imaging (MRI) scan, as well as some non-invasive imaging techniques such as 3D laser scan imaging technique and 3dMD scan system (www.3dMD.com). In addition, continuously renewed research achievements of artificial intelligence (AI) have enhanced the ability of image processing and information processing.

Benefiting from the particular properties of intelligence, objectivity and efficiency, computer aided facial feature analysis applied in medical field has been the subject of intensive investigations of lots of researchers. In this thesis, we closely cooperate with the clinicians from the National University Hospital, Singapore (NUH) for the study related to facial appearance, facial paralysis diagnosis and facial feature analysis.

1.1 Facial paralysis and diagnosis

1.1.1 Facial Paralysis

Facial paralysis (FP) is a condition when the facial muscles' function is weak or complete paralyzed on one or two sides of the face as a result of

Bell's palsy (also termed idiopathic facial paralysis), post-surgical trauma in parotid surgery, skull base tumors or fractures of the temporal bone, however in a lot of cases without known cause.[5] The cosmetic drawback for the patient is clearly visible as shown in Figure 1.1. The patients usually suffer from huge psychological stress along with short-term or long-term disfigurement, difficulty in speaking, eating and drinking, decreased taste in the mouth and reduced tear production from the affected eye. Not knowing the cause, there is no effective treatment to avoid sequelae or persistent palsy in the around 30% of patients who would fail to recover completely.[6]

(a) **(b)** **(c)**

Figure 1.1 Patients with Bell's palsy.[7] (a) Asymmetric elevation of brow and wrinkling of the forehead; (b) Incomplete eyelid closure; (c) Flattened nasolabial fold and poor turning upward of the left side of mouth.

The most common facial paralysis is Bell's palsy, and bilateral facial paralysis is clinically rare. Kevin Tsai, a famous writer and television host in Taiwan, was diagnosed with Bell's palsy previously and almost failed to take up the responsibility as the host and judge for the 50th Golden

Horse Awards.[8] Bell's palsy was named after Sir Charles Bell (1774 - 1842), who first identified the syndrome as well as the anatomy and function of the facial nerves.[9] The annual incidence of Bell's palsy is 15 to 30 cases per 100,000 people, with equivalent amounts of males and females affected. The etiology of Bell's palsy is still under debate. It is usually "believed to be caused by inflammation of the facial nerve at the geniculate ganglion, which leads to compression and possible ischemia and demyelination" (Figure 1.2),[5] Infection with herpesviruses, especially herpes simplex virus type 1 (HSV-1) and varicella-zoster virus (VZV), has gained support as a possible cause.[10]

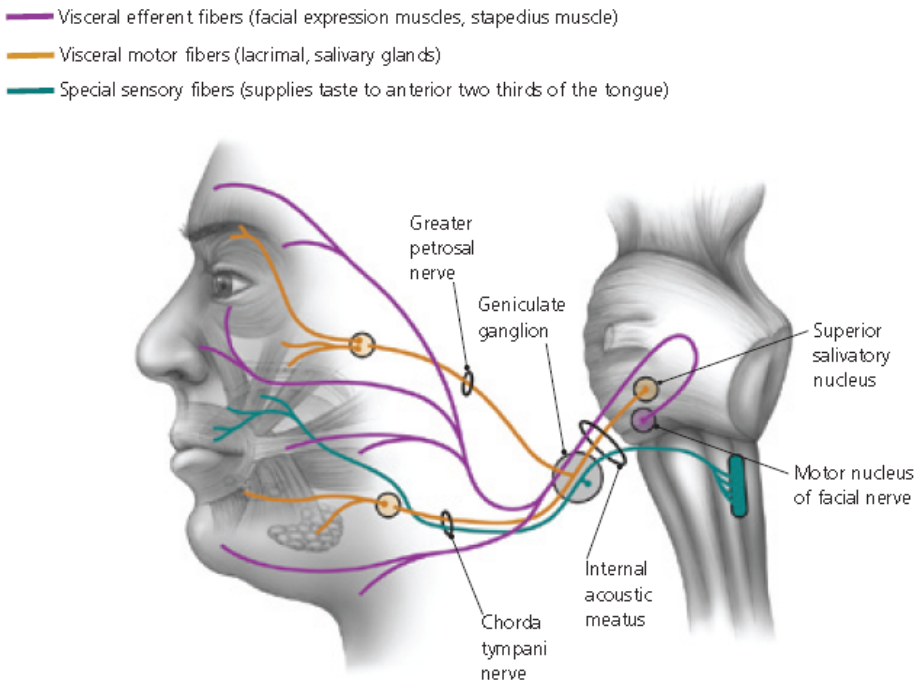

Figure 1.2 Anatomy of the facial nerve.[9]

Grading facial function is required for identifying and confirming the spontaneous course of FP and especially the consequence of medical or surgical treatments. The diagnosis of facial paralysis is usually made based on patient's asymmetric and weak facial presentation while interpreting different facial expressions. However, FP studies are limited by the lack of an objective, standardized evaluation method. The subjectivity of the grading methods leads to intra- and inter-observer variation.[5]

1.1.2 Clinical Facial Paralysis Assessment Methods

A diagnosis of facial paralysis is usually made based on patient's weak or completely lost facial presentation while interpreting a specified series of facial expressions. The most common assessment of the severity of facial paralysis is by the six-grade House-Brackmann grading system (HBGS),[11] which was originally proposed by House,[12] and then soon improved by Brackmann and Barrs.[13] It has been officially adopted as the universal standard of the American Academy of Otolaryngology–Head and Neck Surgery for facial paralysis diagnosis. The patient is requested to perform a series of certain facial movements which will be subjectively assigned a grade of paralysis ranging from grade I (normal) to grade VI (no

movement) by the clinician. The HB grading system is simple to apply and it is able to achieve a single-score description of facial function. The main criticisms are that it relies on a subjective judgment with remarkable inter- and intra-observer variation[14-17] and it is insensitive to local differences of facial movement. For instance, Neely et al.[18] reported that when nine patients were examined by 13 assessors in the study, none of the grades of the patients had 100% agreement, although most of the differences among these assessors were within one grade. In another reported study by Coulson et al.,[17] there was complete agreement of six assessors for only one patient out of the 21 patients in the reported study, one grade apart for 12 patients, two grades apart for six patients, and for two patients, assessments were even three grades apart. Since the HB system is only a gross scale with six grades, even one grade either up or down reflects a considerable difference in facial function. The subjectivity of the evaluation makes it even more difficult to determine the improvement or deterioration of the conditions of the patients after a short time lapse.

There are some other traditional manual classification methods as well. Some methods preferred to provide a more accurate measurement of the disease's severity, such as the facial nerve paralysis grading system of

May,[19] the facial paralysis score of Stennert,[20] the Yanagihara's 40-point scale system,[21] a detailed evaluation of facial symmetry (DEFS) by Pillsbury and Fisch,[22,23] the Sydney facial grading system,[24] and the function level grading scale by Smith et al.[25,26] While these methods may be precise in their diagnosis, they are considered to be too complex for implementation. Some other methods aim to simplify the grading process, such as the Sunnybrook facial grading system (SFGS),[27] the Ardour-Swanson Facial Paralysis Recovery Profile (FPRP) and Index (FPRI).[21,28] However, a patient's condition may be improved or worsen clinically while such variation may not be detected by the grading system. In summary, these methods are all limited by their subjectivity and disparity, although they tend to strike a balance between sensitivity and complexity. Different clinician may grade the same patient differently using the same scale. Therefore, an objective grading system for facial paralysis diagnosis would be desirable.

In this thesis, the SFGS grading method proposed by Ross et al.,[27] was adopted as the reference grading system. It was also named as Toronto Facial Grading System because that the writers, Ms. Ross and Dr. Nedzelsk were from Sunnybrook Health Science Centre Toronto. The evaluation of SFGS is performed by fulfilling a form as shown in Figure

1.3, and addressing a weighted and subjective scale together with incorporation of secondary defects into a single composite score. The first step requires the observer to evaluate the symmetry of the eye, cheek, and mouth at rest with a score of zero to two, and the sum of these three scores is multiplied by five. In the second step, the observer rate facial movements of the patient while doing five standard facial expressions on a scale of one to five. Then, the scores are totaled and multiplied by four. In the next step, in a departure from the yes or no assessment of the Nottingham system, the observer is required to grade the severity of synkinesis on a four-point score for the five facial expressions same as in the second step. From these three scores, a total composite score in the range from 0 for total facial paralysis to 100 for normal function is attained by subtraction of the synkinesis and resting score from the voluntary movement score. It has been proven to have high intra-system reliability and good intersystem association for the assessment of patient facial movement. [17,29]

The HBGS with continuous scale was able to successfully distinguish among finer levels of facial nerve functions before and after rehabilitation treatment of facial nerve injury. On the other hand, this grading system cannot distinguish rehabilitative improvements in facial nerve function.

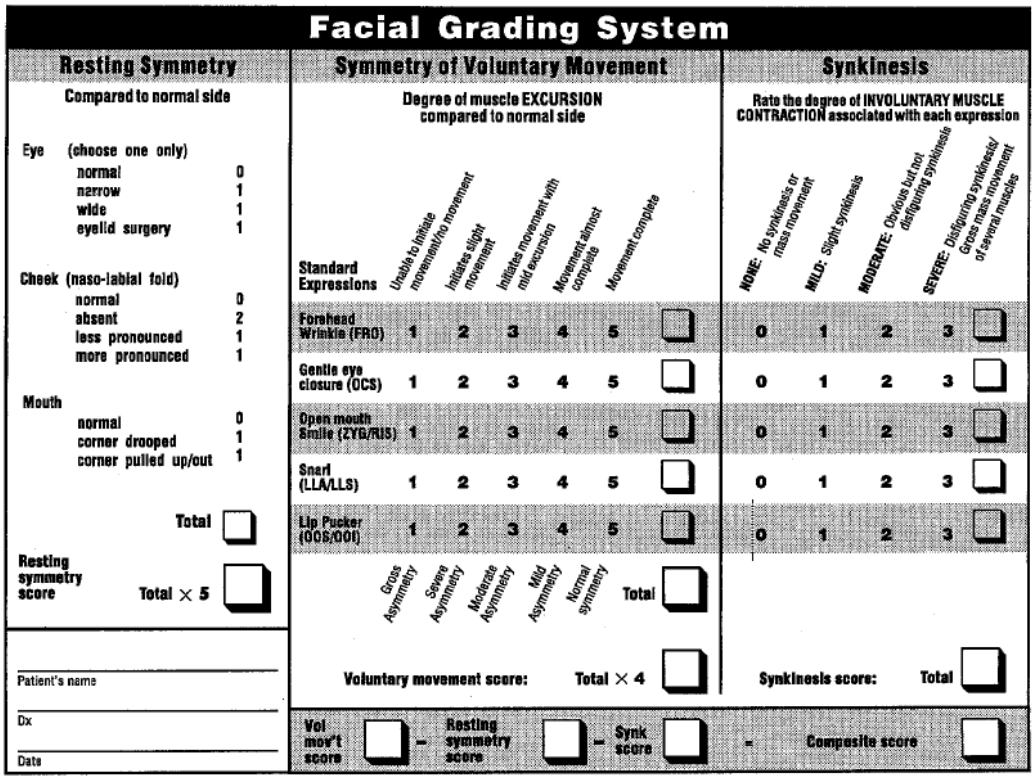

Figure 1.3 SFGS standard form.

1.1.3 2D Image and Video Based Computer Aided Diagnosis

To overcome the shortcomings of subjectivity and disparity in the various manual grading systems, several objective facial asymmetry grading systems have been reported. They are typically based on 2D images or videos focusing on automated analysis of asymmetry of facial features. Apparently, the severity of the patient's condition is closely relevant to the degree of the asymmetry of the face. Several of pioneering works also involve manually placing markers on the face[30-34] to trace the facial movements, or label the feature points on the images. For example,

Wachtman et al.[34] evaluated the severity of facial paralysis by measuring the facial asymmetry for static 2D images. Facial feature points were labeled manually on the images to define the face midline. Although these methods make the image processing simpler, they have relatively poor maneuverability since they need well-trained technicians to accurately and precisely place the markers on the right positions.

Some other automated methods without the use of markers have also been developed. McGrenary et al.[35] and Neely et al.[18] quantified the differences between the images of a video as the measurement of facial paralysis. Wang et al.[36] developed an objective facial paralysis grading method based on P_{face} and eigenflow on the static pictures of voluntary expressions of a patient. P_{face}, which stems from a human identification index, is a facial asymmetry measurement between two sides of the face. Eigenflow is a measurement of the expression variation between the patient and normal subjects. He et al.[37] presented an approach automatically analyzing patient video data, which would need to manually define the relevant facial regions. However, 2D image and video acquisitions are the projection process from 3D to 2D space, which definitely causes information loss. Compared to traditional 2D images or videos, three-dimensional (3D) images retain more information of local

contour, and thus should be introduced to the facial contour analysis work. Some of these methods also analyze the difference of radial coordinates between opposite points in cylindrical coordinate system, and thus require an accurately set reference coordinate system.

In summary, although facial paralysis is a 3D problem, most reported works on the development of computer based objective grading system for facial paralysis are based on 2D images or videos. Few studies have applied the 3D technology which provides more local contour information of the face. Moreover, few reported works have examined the sensitivity of the proposed grading system for the evaluation of improvement or deterioration of the proposed objective grading systems.

As a result, lots of practitioners have considered computer-based 3D technologies, which offer surgical professionals with more contour information than mere 2D images. This is in view of the fact that details are lost while projecting a 3D object to 2D, and 3D models are also not susceptible to the lighting condition variation or camera pose. Moreover, advanced 3D scanners are characterized by their convenience, portability, non-invasiveness, precision, and accuracy, and the adoption of 3D

technology to aid plastic surgeons will avoid uncertainty and subjectivity which is inherent to current analysis techniques.

All the objective facial paralysis diagnosis studies reviewed above suffered from a serious limitation in that they rely on manually setting the landmarks. Meanwhile, there is still a huge potential of untapped 3D techniques for facial mesh asymmetric analysis. The specific gaps relates to facial paralysis diagnosis are:

1) To overcome the subjectivity of the traditional diagnosing methods, current works in this area are mainly based on locating the landmarks and evaluating the movement of these landmarks throughout the subject's facial movements. Apparently, the process of placing landmarks requires technicians to be well trained. This is also a subjective process itself. So far, there is still a requirement for developing objective diagnosis systems.
2) Although 3D image has been introduced in some facial paralysis diagnosis studies, they are simple extensions from 2D to 3D. The traditional 2D methods are transferred directly to 3D methods. There are various 3D surface based measurements and algorithms, which have not been applied on this topic.

1.2 Facial highlight Features Analysis

The face region would be the primary visual identifier of a human being, and it carries remarkable significance of biological vitality and aesthetic beauty or as a way of communication through various facial expressions. Given the importance of the face, it is no wonder that all through the mankind history, attempts have been made not only to observe and to

Figure 1.4 Comparison of two pictures with Andie MacDowell in different ages.

record the facial features, but also to generalize and to uncover the principles. Ancient Greeks were known to study facial dimensions using classical geometry, and some others, like D'Arcy Thompson, applied mathematical analysis to the patient observation of biological phenomena.[38]

At the same time, more and more modern plastic surgeries are taken not only to correct the facial abnormality, but also to improve the aesthetic appearance of the face. The characterization of the individual face is a primary activity of a plastic surgery, whose role is usually to reconstruct the appearance of the face for restorative or aesthetic purposes. The surgery is to enhance facial harmony by reshaping the patient's face with prosthetic implant or filler injection. Even one minor corrective surgery may have a dramatic effect to the way people look and feel. Recently, soft tissue deflation also has been recognized as a key component of facial aging. With the advent of non invasive surgery, the restoration of facial volume via fillers has been increasingly popular. Figure 1.4 shows one example of how the volume losses and the highlight changes on the face of a celebrity as the time passed, and it is believed that she had cosmetic surgery and injected Botox to improve the appearance.[39] Where shall we refill the volume? Apparently, it is essential for surgical procedures to

identify the desirable facial profile, a beautiful and natural one. To determine the appropriate surgical intervention, surgical analysis should be based on different ethnic descent and accepted cultural standards.[40]

Historically, science and medicine have tried to quantify facial features in its own terms with some repeatability and reliability. The neoclassical canons of Leonardo da Vinci were one of the first attempts to define the proportions of human body and head[41] (Figure 1.5). In more recent times, Leslie G. Farkas – a plastic and reconstructive surgeon – has defined the field of facial anthropometry, describing countless soft tissue measurements to characterize the face.[42] Quite a few studies investigating facial standards have been carried out on defining angles and proportions of the facial features. For example, Jefferson studied the aesthetics significance of divine proportion (1.618, also known as golden ratio) as a universal standard for facial beauty.[43] Gunes and Piccardi found the strong central tendency of the perception of universal human facial beauty based on a survey of diverse human grading a group of female facial images.[44] Specially, Woodard and Park analyzed the aesthetic facial and nasal proportions in people of different ethnic descent.[45] Significant social science literatures have attempted to identify the objective factors which

describe faces of different race and gender. These works tend to focus on bone cuts and movements and their effect on profile change.

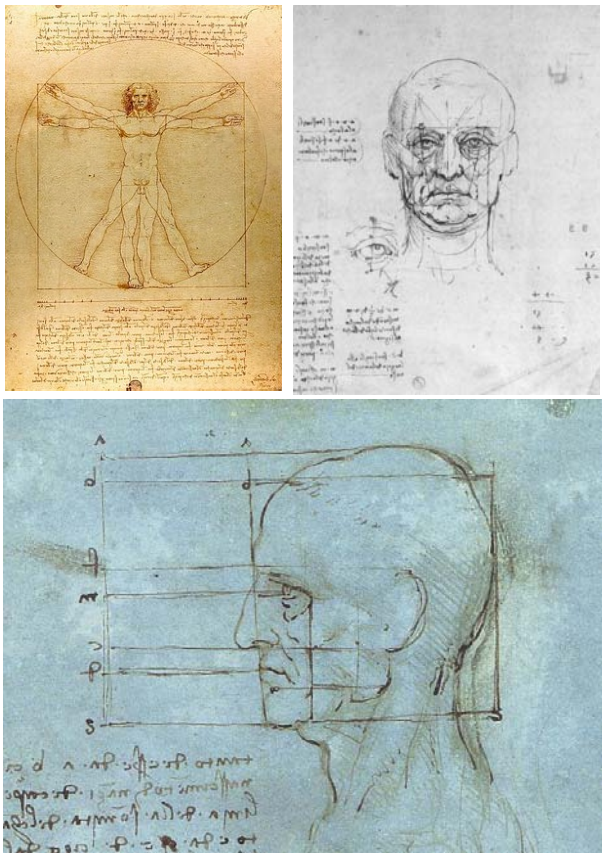

Figure 1.5 Study of the proportions of human body and head by Leonardo da Vinci.

Besides symmetry, proportions, and angles, which are more convenient to be objectively measured, some other facial features, the shape and position of the highlight regions have also been recognized as key components of facial appearance. The highlight regions are what the eyes will focus on at the first sight. It has been a long time since the make-up

artists found the secret of highlighting and contouring with foundation or powder that could bring new dimensions to the face. The highlight color is usually applied on the forehead, on the nasal bridge, at the top of the cheekbones, or the tip of the chin (Figure 1.6).[46] For example, creating the illusion with some highlight powder over the nasal bridge may make the nose looks long and straight and thus improve the appearance of the face. However, according to our literature review, researchers have not treated facial highlights in much detail. Data is still missing on where these highlights should be on natural faces, especially on faces of different ethnic descent and gender. Such knowledge may assist cosmetic surgeon in making surgery plan and make the face appear natural.

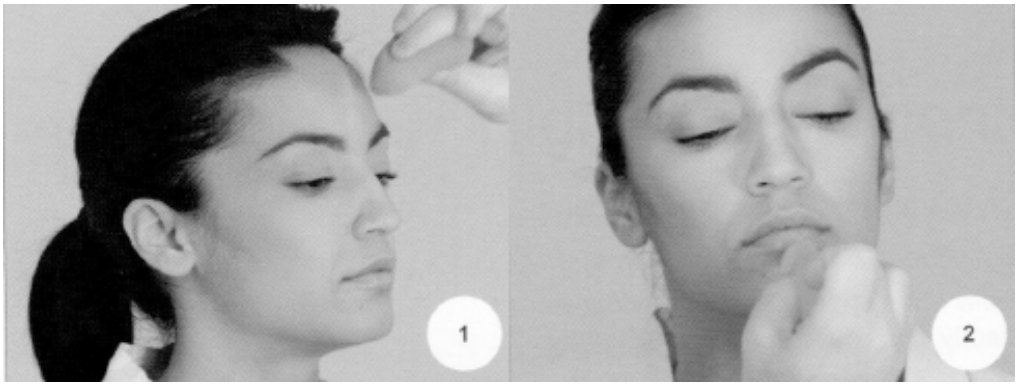

Figure 1.6 Makeup expert applies highlight foundation on the face of the model, and tries to enhance the facial features.[46]

Traditional surgical planning is based on subjective opinion of the surgeons, which is not quite reliable. In this study, objective facial highlight and contour feature analysis by means of 2D and 3D image technologies are carried out to assist surgeons on operation plan designing. So far, very few works have been carried out in this area.

1.3 Objectives of the Thesis

The proposed study aims to develop an automated objective asymmetry grading system for facial paralysis diagnosis (Figure 1.7) combining higher order surface properties for 3D model local contour description, artificial neural networks (ANNs) for classification of the subjects. In this system, 3D models of the human face with different facial expressions are first reconstructed. Second, higher order properties of each point are calculated as descriptions of the surface local features for grading the asymmetry of the faces. After that, the original surface and its mirror one are superimposed by the ICP algorithm and compared to evaluate the asymmetry degree of the face. The comparison result is quantified by several indices as the input of an ANN. The trained ANN is then expected to output a diagnosis result of the facial paralysis patient. Overfitting frequently occurs when high-dimension and small-size sample set is

applied while training neural network. Thereafter, noise injected neural networks are used to improve the performance of the classifier. A large number of previous studies have shown that injecting noise to the input data can improve the ANN's generalization ability.[47,48]

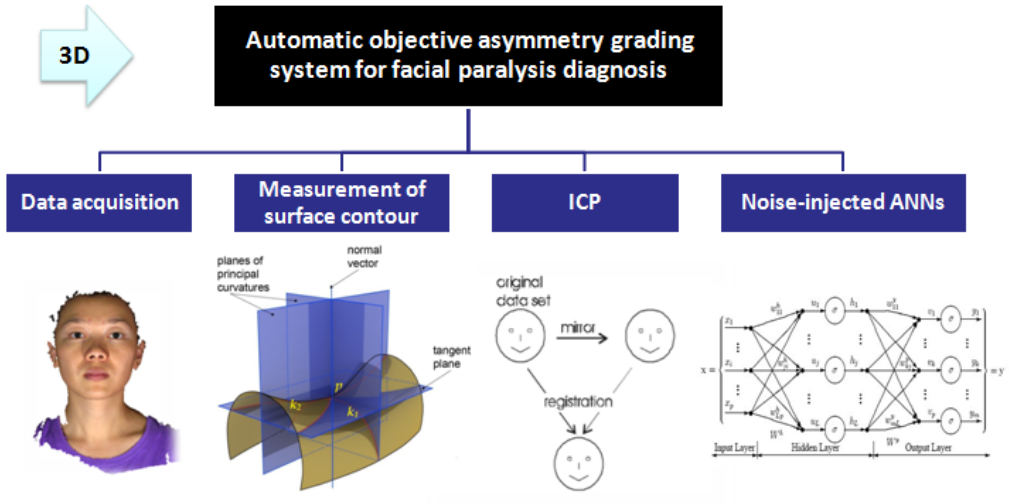

Figure 1.7 Overview of the objective asymmetry grading system

1.4 Overview of the Thesis

In this chapter, an introduction to facial paralysis, some clinical assessment methods, and previous facial feature studies has been given, followed by the objectives and organization of the thesis.

In Chapter 2, an introduction of some concepts and methods related to this study, including 3D curvatures for surface local contour measurement,

iterative closest point method for 3D surface matching, and artificial neural networks for classification are given.

Chapter 3 describes an objective facial paralysis diagnosis system developed in this study. 3D curvatures and shape index are introduced in for grading the severity of facial asymmetry. Noise injected neural networks are applied to reduce the overfitting effect and improve the classifier's performance.

In Chapter 4, the facial highlight features are studied. The study focuses on the positions and schemas of the facial highlight regions, as well as the difference among the race and gender factors.

Finally, some closing remarks are given in Chapter 5.

Chapter 2. Methodology

2.1 3D Curvatures

We've gained much from the improved 3D images reconstruction techniques and the 3D curvatures of a surface are now able to be easily calculated. These curvature measurements are found in studies on facial feature detection and automatic face recognition.[49,50] Salient face features, including the eyes and nose, are detected with a research into the curvature on the surface. However, there is no known previous study on facial deformity or attractiveness that experimented with incorporate measurements using curvature.

Curvatures measure the degree of a curve or surface bends at one point. In 2D space, the osculating circle is the one among all the circles that tangent to a curve C at point p that most closely approximates C near p. The curvature of C at p is defined as the reciprocal of the osculating circle's radius R.

$$K = \frac{1}{R} \qquad 2.1$$

In 3D Euclidean space, the degree of the surface S bends at a point p in different directions can be measured by curvatures of this point.

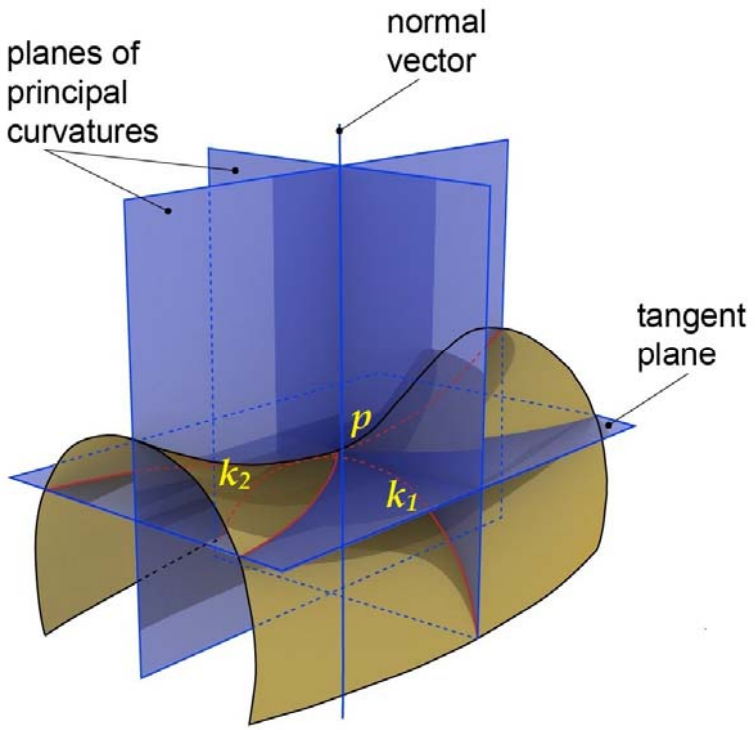

Figure 2.1 Normal planes in directions of principal curvatures of a saddle surface.[51]

At any point p on a differentiable surface in 3D Euclidean space, and any chosen unit vector from point p, the normal plane at point p which contains the chosen vector can be determined. The normal plane determines a direction that is tangent to the surface at point p, and cut this surface with a plane curve. Generally, this curve has different curvatures for different normal planes at point p. The normal curvature at p is defined

as the curvature of the 2D curve, which is the reciprocal of the osculating circle's radius along the desired direction. Then, the principal curvatures at point p, which denoted by k_1 and k_2, are defined as the maximum and minimum values of the curvature (Figure 2.1). The mean curvature H is defined as the average of the two principal curvatures.

$$H = (k_1 + k_2)/2 \qquad 2.2$$

Gaussian curvature K is defined as the product of the two principle curvatures:

$$K = k_1 * k_2 \qquad 2.3$$

Curvatures of point p on a surface measure the degree of the surface bends in different directions at this point. The signs of the curvatures describe the shape of the surface. To take the principal curvatures for example, at elliptical points, both have the same sign, and the local surface is convex; at hyperbolic points, the two principal curvatures will have opposite signs, and the local surface will be saddle-shaped; at parabolic points, one of the principal curvatures is zero. Parabolic points usually lie in a curve which separates hyperbolic and elliptical regions. These properties of the principal curvatures can be used on the study of nasal bridge feature.

Gaussian curvature K is also frequently chosen for being an index of quantified contour due to its ability of well describing the neighborhood contour on the surface along with only one value. It is considered as one of the most widely used indicators for surface shape classification. At point p, if $K > 0$, the contour of the surface is dome shaped. If $K < 0$, the contour of the surface at point p is saddle shaped. If $K = 0$, the surface is parabolic.

There is another shape scale known as the Shape Index (*S.I.*) that was proposed by Koenderink [52]. The Shape Index scale was originally defined by the principal curvatures using the equation:

$$S.I. = \frac{2}{\pi} arctan \frac{k_2 + k_1}{k_2 - k_1} \quad (k_1 \geq k_2) \tag{2.4}$$

It maps the 3D shapes on the segment of [-1, +1]. In order to prevent interaction of attributes and loss of information, Dorai [53] redefined the index to a positive range of $S.I. \in [0,+1]$ as followed:

$$S.I. = \frac{1}{2} - \frac{1}{\pi} arctan \frac{k_2 + k_1}{k_2 - k_1} \tag{2.5}$$

The Shape index also quantitatively measures the shape of a local surface, such that all manners of curved surfaces can be characterized by it (Figure

2.2). Unlike mean curvature and Gaussian curvature, each Shape Index value refers to a unique shape, such as a spherical cap (*S.I.* = 1.0), or saddle (*S.I.* = 0.5). Table 2.1 indicates the different surface shapes and their corresponding principal, mean and Gaussian curvatures, and the Shape index.

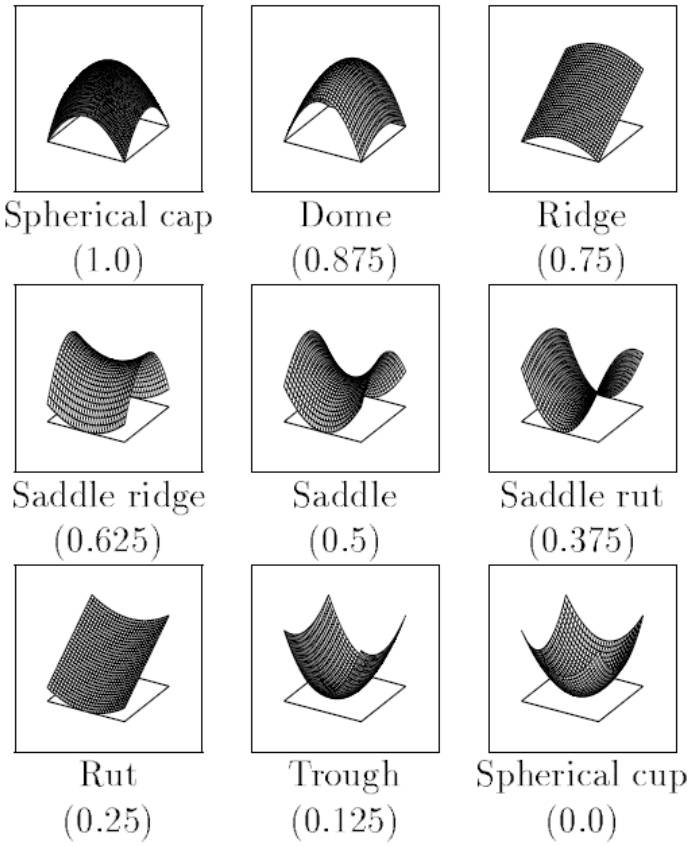

Figure 2.2 The Shape index as a shape descriptor for different shape of surface[53].

Table 2.1 Surface shapes and their corresponding principal, mean and Gaussian curvatures, and the Shape index[53].

Shape	k_1	k_2	H	K	$S.I.$
Concave (Cup)	**-**	**-**	**-**	**+**	**[0, 0.1875]**
Parabolic (Rut)	**0**	**-**	**-**	**0 / -**	**[0.1875, 0.3125]**
Hyperbolic (Saddle)	**+**	**-**	**+ / 0 / -**	**-**	**[0.3125, 0.6875]**
Parabolic (Ridge)	**+**	**0**	**+**	**+/0**	**[0.6875, 0.8125]**
Convex (Cap)	**+**	**+**	**+**	**+**	**[0.8125, 1]**
Plane	**0**	**0**	**0**	**0**	**N/A**

Both curvatures and *S.I.* are translation invariant and rotation invariant. Although *S.I.* is also scale invariant, curvatures are not, and normalization operation is necessary to adjust the measurements to a common scale before analyzing and comparing different subjects.

To derive the curvatures and *S.I.*, we have adapted a rather robust and accurate approach based on a surface patch fitting method in this work.[54,55] Since the mesh is only a discrete representation of real surface, to evaluate the contour at a particular point on the mesh, a local surface geometry was fitted to the region by an osculating paraboloid represented by a quadratic polynomial. Thereafter with the coefficients of the fitting surface, the curvatures can be calculated by the theory of differential geometry.

In the neighborhood of a point x, the local surface can be approximated by an osculating paraboloid that may be represented by a quadratic polynomial with du and dv, where u and v are the parameters of the underlying geometry. This polynomial can be represented as a Taylor expansion at the point x of the paraboloid surface, by omitting the higher order terms of the quadratic term:

$$x(u+du, v+dv) = x_{00} + x_u du + x_v dv + (x_{uu}du^2 + 2x_{uv}dudv + x_{vv}dv^2)/2 \qquad 2.6$$

The coefficients x_{00}, x_u, x_v, x_{uu}, x_{uv} and x_{vv} represent the zero, first and second derivatives of x with respect to u and v at the surface point $x_{00} = x(u, v)$. Then, the curvatures of the surface could be computed with these six derivatives. A function of $z = f(x, y)$, which is a second order polynomial of the form

$$z = c_1 + c_2 p + c_3 q + c_4 p^2 + c_5 pq + c_6 q^2 \qquad 2.7$$

is used to fit the approximating surface region. $p = x - x_0$ and $q = y - y_0$, where x_0 and y_0 are the x and y coordinates of the center point x_0 of the local surface geometry under consideration. In this way, the six coefficients of the paraboloid can be calculated by the least-squares solution of an over-determined system of linear equations:

$$\begin{Bmatrix} z_1' \\ z_2' \\ z_3' \\ \vdots \\ z_n' \end{Bmatrix} = \begin{bmatrix} 1 & p_1 & q_1 & p_1^2 & p_1 q_1 & q_1^2 \\ 1 & p_2 & q_2 & p_2^2 & p_2 q_2 & q_2^2 \\ 1 & p_3 & q_3 & p_3^2 & p_3 q_3 & q_3^2 \\ \vdots & \vdots & \vdots & \vdots & \vdots & \vdots \\ 1 & p_n & q_n & p_n^2 & p_n q_n & q_n^2 \end{bmatrix} \begin{Bmatrix} c_1 \\ c_2 \\ c_3 \\ c_4 \\ c_5 \\ c_6 \end{Bmatrix} \qquad 2.8$$

where n is the number of nearby points in the neighborhood of a selected surface point, and the coefficients c_i are obtained by .

It is desired that the coefficients c_1~c_6 are obtained in ways that the divergence with the fitted paraboloid as well as the data points are

minimized, which is comparable to minimizing the differences between z_n (measured z value) and z'_n (calculated z value). The minimization issue at the desired point is then expressed with regard to error function *E*, as

$$E(z) = \sum_{n=1}^{N} G_n(z_n' - z_n)^2 = \sum_{n=1}^{N} G_n(z(p_n, q_n) - z_n)^2 \qquad 2.9$$

Where *N* represents the amount of points in the fitted paraboloid, and *G* is acquired from a distance weighting function as follows:

$$G_i = f\left(e^{\left(-\frac{p_i^2+q_i^2}{d^2}\right)}\right), i = 1, 2, 3, \ldots, N \qquad 2.10$$

where *f* and d are arbitrary constants that could be adjusted accordingly. The error function E may reach to a minimum when

$$\frac{\partial E}{\partial c_i} = 0, \qquad i = 1, 2, 3, 4, 5, 6 \qquad 2.11$$

thus variant six linear equations needed to calculate the six coefficients.

The coefficient c_1 is the z value of the central point x_0 of the fitting surface patch, and the other five coefficients c_2~c_6 could be interpreted as the first and second derivatives of x regarding to p and q at x_0. Using these coefficients, the principal curvatures k_1 and k_2 can be easily derived with the theory of differential geometry.[56,57] The normal curvature at that point is then calculated as

$$k(\lambda) = \frac{L + 2M\lambda + N\lambda^2}{E + 2F\lambda + G\lambda^2} \qquad 2.12$$

where $\lambda = dv/du$, such that u and v are the parameters of the underlying geometry, and $\{E, F, G\}$ and $\{L, M, N\}$ are components of the first and second fundamental forms, respectively. The extreme values k_1 and k_2 of $k(\lambda)$ are the maximum and minimum principal curvatures, respectively, and they are obtained from the roots of the equation:

$$det\begin{bmatrix} L - kE & M - kF \\ M - kF & N - kG \end{bmatrix} = 0 \qquad 2.13$$

2.2 Iterative Closest Point

The Iterative Closest Point (ICP) algorithm is a widely adopted solution to the surface alignment problem. This algorithm firstly proposed by Besl and McKay[58] is intended to minimize the difference or distance between two clouds of points. ICP is frequently employed to reconstruct 2D or 3D surfaces from several scan pieces, to localize robots and optimize path planning (particularly when wheel odometry is unreliable because of slippery terrain), etc. In this work, ICP is applied to superimpose the original and mirror meshes for evaluating the asymmetry degree of the face. The algorithm is conceptually efficient and is frequently employed in

real-time applications. The main idea of the algorithm is to iteratively revises the transformation (translation, rotation) and minimize the amount of the distance between the paired points of two scan pieces.

This algorithm aims to solve the problem of Euclidean alignment of two or more roughly pre-registered, especially overlapping 3D point clouds with measurement outliers and, perhaps, contour defects. This issue has been primarily considered in 3D model acquisition (scene reconstruction, reverse engineering) and motion tracking and analysis, including model-based tracking. Given two 3D point sets with coordinates, *P* and *M*, the aim is to find the Euclidean motion that transfer *P* to the best possible alignment position with *M*.

The ICP algorithm has three main steps:

1. For each point of *P* find the closest point in *M* by the nearest neighbor criteria by means of the *k-d* tree[59] to make a pair;

2. Compute the motion parameters (the parameters of shift and rotation) using a mean square cost function to minimize the mean square error (MSE) between the paired points;

3. Apply the motion using the estimated parameters of step 2 to *P* and update the MSE.

These three steps are iteratively applied. It has been proven that the iterations converge in terms of the MSE.

The concept of ICP has been proven very effective in view of the fact that it was implemented by many applications, improvements and modifications. Pulli,[60] Rusinkiewicz and Levoy[61] provided comprehensive surveys oriented towards range images that offer a summary of the variants of the ICP algorithm. They categorize the variants based on the way the algorithms: (1) select subsets of point sets *P* and *M*; (2) match points to pairs; (3) weight the pairs; (4) reject pairs; (5) assign error metric; (6) reduce the error metric.

2.3 Artificial Neural Network

Artificial neural networks (ANNs) are a well known artificial intelligence technology that intends to mimic the mechanism of the brain and nervous system. The structure and operation of ANNs have been described by many authors[29,62-65]. Here is one definition: "A neural network is a massively parallel distributed processor made up of simple processing

units, which has a neural propensity for storing experiential knowledge and making it available for use."[66] Generally, ANNs comprises a number of neurons (also called nodes or processing elements (PEs)) that are normally connected and arranged in layers. A typical ANN has three layers: an input layer with input neurons, an output layer with output neurons, and one or more hidden layers[67] (Figure 2.3). Signals are transferred from neurons of lower layers to the ones of higher layers through the connecting links. The neurons in the same hidden layer may also be connected. Neural networks with a large number of nodes are frequently used since they are sufficient for many nonlinear practical problems.

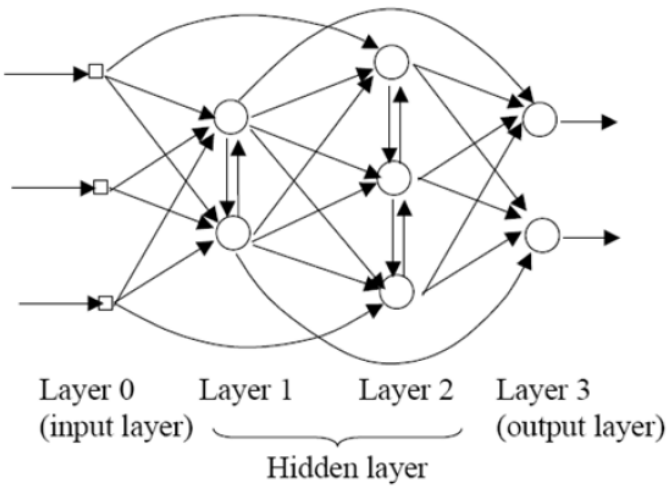

Figure 2.3 Architecture of Artificial neural network

For each neuron k, the input signals (stated as some numerical values) from the previous neurons x_i are multiplied by the adjustable synaptic weights w_{ki} that characterize the connecting links, and then are summed and a bias value b_k is added by a linear combiner. This combined input v_k is then passed through a non-linear activation function $\phi(.)$ to limit the amplitude range of the output signal (typically [0, 1] or [-1, 1]) and produce the output of the neuron y_k. The output of one neuron may provide the input to the neurons next to it, or the output of the neural network. This process is described in Figure 2.4 and illustrated in Equation 2.14 and 2.15.

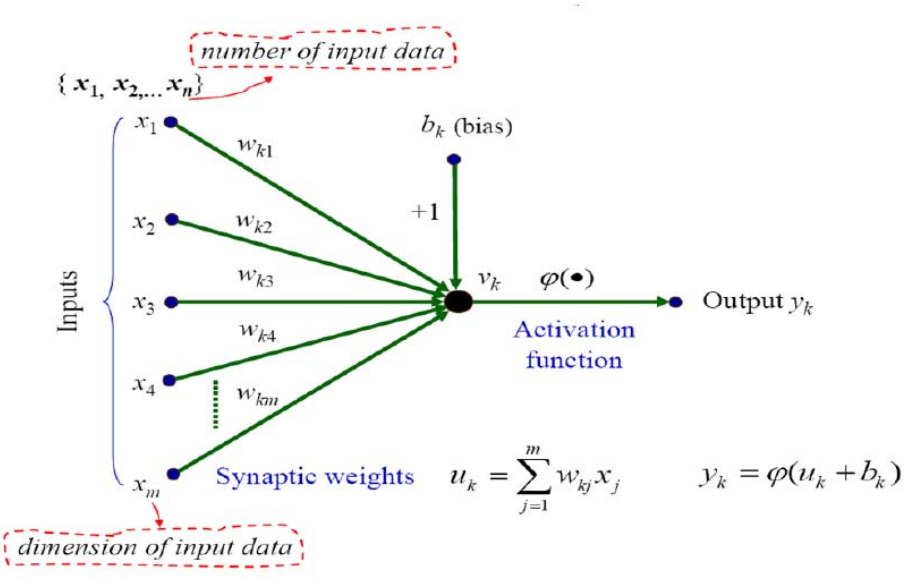

Figure 2.4 Model of a neuron *k*.

$$v_k = \sum_{j=1}^{m} w_{kj} x_j + b_k$$

summation *2.14*

$$y_k = \varphi(v_k)$$

activation *2.15*

A single layer neural network is called perceptron, and is only able to solve linearly separable classification problem and linear regression problem. However, a neural network combining a number of perceptrons is capable of solving a considerable number of complex and highly non-linear problems. Multilayer perceptron (MLP) networks with feedforward connections as shown in Figure 2.5 are most commonly used networks. Neurons of the networks receive the output signals of the preceding layer as their input signals only, and there is no connection between the neurons in the same layer. There may be one or more layers in the hidden layer. Generally, each neuron adopts a nonlinear (differentiable) activation function, such as logistic function:

$$y_j = \frac{1}{1 + exp\,(-v_j)}$$

2.16

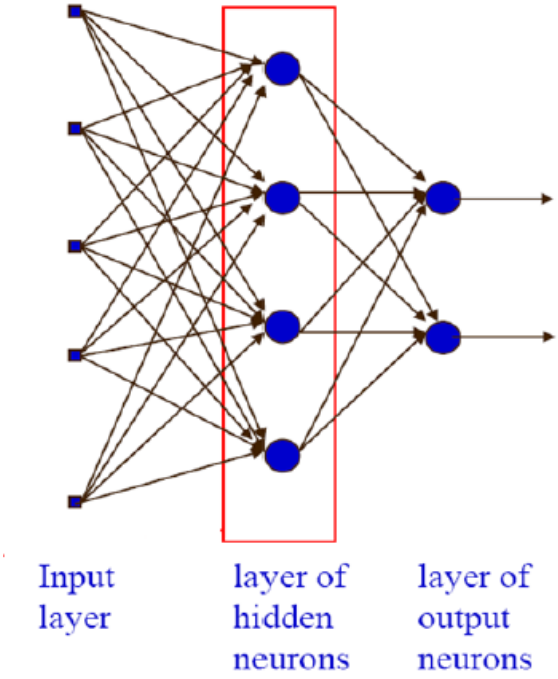

Figure 2.5 Architectural graph of multilayer perceptron feedforward networks.

Once the structure of the neural network is determined, the neural network will go through a process called "learning" or "training". The neural network is iteratively fed with training data that describes the desired input/output mapping. The free parameters of the network are adjusted in each epoch according to the error signal that is the difference between the desired and actual outputs. The training method determines how the parameters change and when the learning process stops. Back-Propagation (BP) algorithm is a common method of training neural networks that will also be used in this thesis. Different from the direction

of function signals, the error signal is propagated back from the output layer to the input layer. There are two alternate passes of computation in each epoch:

1. Forward pass: Computation of function signals for each neuron.

2. Backward pass: Starts from the output layer, recursively calculate the error signal δ for each neuron beginning with the output layer towards the first hidden layer. At each layer, the synaptic weights w_{ki} are updated accordingly. Suppose in the n^{th} iteration, the MLP is fed with an input $x(n)$, and produces an output vector $y(n)$, and $d(n)$ denotes the desired neural network output,

$$y_j(n) = x_{out,j}^{(3)}(n) = \varphi^{(3)}(v_j^{(3)}(n)) \qquad 2.17$$

$$w_{ji}^{(s)}(n+1) = w_{ji}^{(s)}(n) + \eta\delta_j^{(s)}(n)x_{out,i}^{(s-1)}(n) \qquad 2.18$$

Where

$$\delta_j^{(s)}(n) = (d(n) - x_{out,j}^{(s)}(n))\varphi^{(s)\prime}(v_j^{(s)}(n)) \qquad \textit{for output layer} \qquad 2.19$$

or

$$\delta_j^{(s)}(n) = (\sum_{k=1}^{n_{s+1}} \delta_k^{(s+1)}(n)\, w_{kj}^{(s+1)}(n))\varphi^{(s)\prime}(v_j^{(s)}(n)) \quad \textit{for hidden layer} \quad 2.20$$

The training phase usually stops when the mean squared error signal is less than some desired threshold value, or the free parameters of the network are stable. When the training phase of the network is successfully completed, the performance of the trained model needs to be validated using a testing set independent with the training set. [68-70]

As described above, ANNs learn from the examples from training data set presented to them and attempt to learn the "behavior" of the data set, or the relationship between the input and the corresponding outputs. Therefore, compared to most statistical and empirical methods, ANNs do not need any prior knowledge about the nature, which is one of the advantages that ANNs have.

In the real applications, the problems are likely to be complex and highly non-linear. Usually, traditional regression analysis method is not adequate.[71] On the contrary, ANNs can be used to solve this complexity by altering the transfer function or network structure, and the type of non-linearity can be changed by varying the amount of hidden layers and the amount of nodes in each layer. Furthermore, both the number of input and that of output nodes are variant.

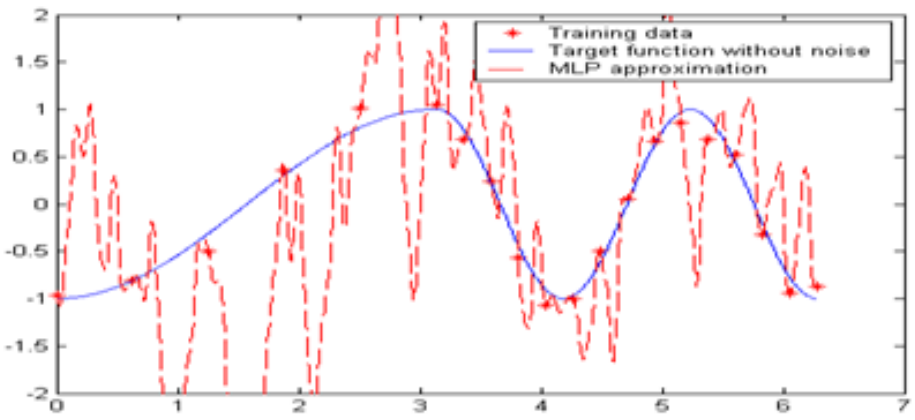

Figure 2.6 Overfitting occurs when excessive number of nodes is used in the MLP neural network.

A trained neural network is expected to generalize well for test data. The performance of the network depends not only on the size and accuracy of the training set, but also the conformability of the network structure. A simple network structure might not be sufficient to fit the data; on the other hand, overfitting may take place if the complexity of the target problem is overestimated.[72] As shown in Figure 2.6, the neural network learns the random error or the noise in the training data instead of the real relationship and results in poor predictive performance. Generally, with an error of 10% the number of training examples needed should be about 10 times the number of free parameters in the network.[73] Overfitting may be overcome with optimized network structure, and improved training strategy. Noise injected neural networks have been proven that they are

capable of reducing overfitting to a great degree.[74] It will be described in a subsequent chapter, and applied in this study.

Chapter 3. Objective Grading System for Facial Paralysis Diagnosis

3.1 Overview

The proposed study aims to develop an automated objective asymmetry grading system of facial paralysis diagnosis combining higher order surface properties in facial imaging technique for 3D model imaging and reconstruction, artificial neural networks (ANNs) for data mining in terms of feature extraction and classification for the 3D subjects. Higher order properties are introduced for grading the asymmetry of the faces as descriptions of the surface local features. Overfitting is a serious problem that high dimension small-size sample set would typically encounter in training neural network. In order to avoid overfitting, noise injected neural networks are applied in this study to improve the classifier's performance. A substantial number of previous studies have shown that injecting noise to the input data can improve the ANNs' generalization ability.

More specifically, the objectives of this work were:

1) To combine higher order surface properties in facial imaging technique for 3D model analysis by specifically considering 3D principle curvatures and Gaussian curvatures.
2) To achieve facial symmetry grading based on the comparison between the original and mirror facial mesh after fine registration by the iterated closest-point algorithm (ICP), which does not rely on any landmarks.
3) To achieve small sample set feature extraction and classification for 3D objects by noise-injected neural network.

This present study should provide a landmark-independent method for evaluating the degree of facial paralysis. Higher order surface measurements such as 3D curvatures describe local contour of the surface rather than simply provide the position. So this work is expected to improve the diagnosing performance compared to previous 3D based works.

The program was developed using MATLAB (version 7.10.0 (R2010a), The MathWorks Inc., Natick, Massachusetts, 2010) and Visual C++ under Microsoft Visual Studio 2005 environment.

Bell's palsy is the most common condition of facial paralysis, which covers all of the conditions except for cases caused by brain tumor, stroke, and Lyme disease. Meanwhile, only rare cases (1%) of facial paralysis occur bilaterally resulting in total facial paralysis.[75] Hence, like previous studies, we focused on unilateral facial dysfunction caused by Bell's palsy. The other few conditions were not considered.

3.2 Data acquisition

In this study, a 3dMDface system (www.3dMD.com, Figure 3.1) was used to produce 3D facial meshes with texture of the individuals. This multiple camera photogrammetry system with structured light patterns takes non-invasive photographs from different viewpoints simultaneously and reconstructs them as a 180-degree face (ear-to-ear) mesh with texture.[76] This system has two sets of three cameras (one color and two infrared) on each side of the photographed subject. A random light pattern is projected onto the subject, and images are captured in 1.5 milliseconds by these synchronized digital cameras precisely set in an optimum configuration. Thereafter, the 3D image is reconstructed as a triangulated polygon mesh (Figure 3.2) by calculation based on the difference of the images captured

from different angles. The meshes are composed of vertices, edges, and triangular facets.

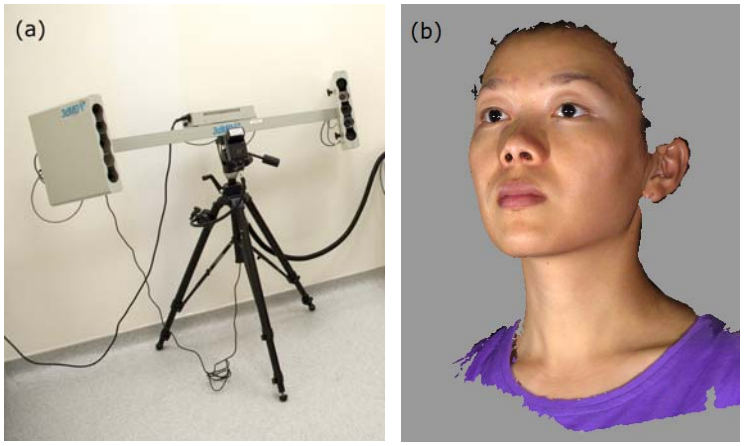

Figure 3.1 (a) 3dMDface system and (b) reconstructed 3D image.

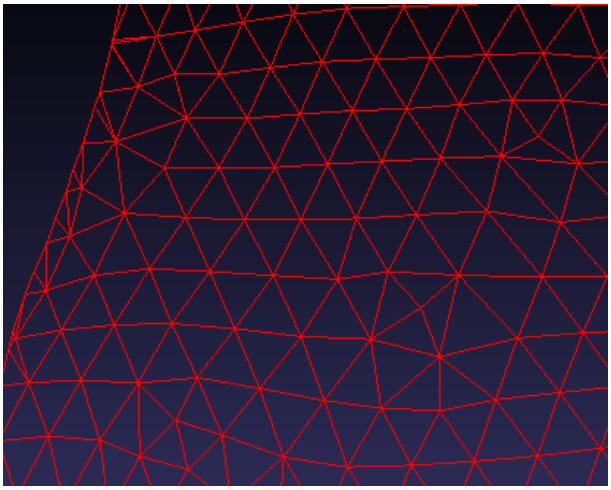

Figure 3.2 Detail of triangulated polygon facial mesh.

Each image file is kept in the form of a triangular mesh, which consists of x-,y-,z- coordinate triples of the points (scanned locations of the surface), and a list of triangles (plane segments) that connect these points. The triangle mesh representation method is widely used as a piecewise linear approximation to the real surface of the object in 3D Euclidean space. The raw data may contain approximately 200, 000 mesh points and 250, 000 triangles for each subject. The meshes need to be normalized with respect to user-selected landmarks on the face.

3D image data of eight single-side facial paralysis patients and twelve normal subjects were obtained in the Department of Otolarygology, Head and Neck Surgery, National University Hospital of Singapore (NUH). Approval from the relevant Institutional Review Board (IRB) had been obtained prior to the study. The patients have been diagnosed as Bell's palsy by clinicians based on the SFGS.[29,77] SFGS is a physician based score instrument. The patient face is assessed with 5 standard expressions, and graded with a composite score in the range from 0 for total facial paralysis to 100 for normal function. It has been proven to have high intra-system reliability and good intersystem association for the assessment of patient facial movement[17].

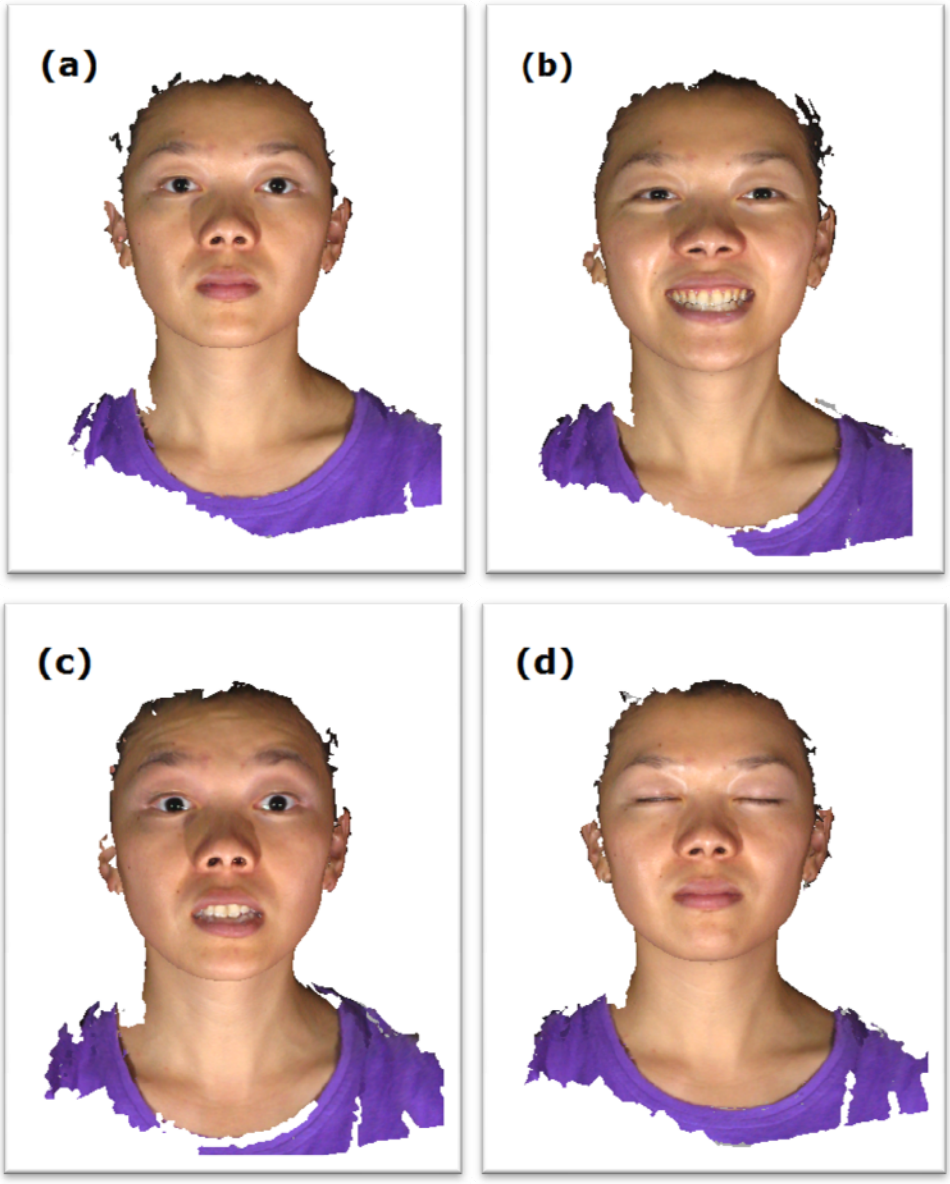

Figure 3.3 3D models of face acquired by 3dMD system for four different expressions: (a) straight and natural stare, (b) smiling to show teeth, (c) raising eyebrow to wrinkle forehead, and (d) closing the eyes tightly.

Five out of the eight patients in the study were also involved in the follow-up studies during the subsequent treatments. For each subject, four models were obtained while they were asked to form four different

expressions: namely, eyes straight and natural stare, smiling to show teeth, raising eyebrow to wrinkle forehead, and closing the eyes tightly (Figure 3.3). These meshes were then trimmed to facial oval region only, excluding hairline, ears and neck. The abnormal muscle functions of the patients would cause facial asymmetric response.[9] We aimed to evaluate the facial asymmetry degree as the objective diagnoses of facial paralysis.

3.3 Objective Measurement of the surface contour

Since 3D images were collected, we were able to introduce in 3D curvatures, the second-order descriptions of the local surface contour for further analysis. In previous reported studies, these factors have not been introduced for the grading of the asymmetry of the faces. In this study we have adapted a rather robust and accurate approach based on a surface patch fitting method as described in Chapter 2 to derive the curvatures.[54,55] In the vicinity of point *P*, the surface is approximated by an osculating paraboloid, which is represented by a quadratic polynomial. Thereafter with the coefficients of the fitting surface, the principal curvatures, the Gaussian curvature, and the Shape Index can be directly calculated by the

theory of differential geometry. The program was developed using Visual C++ under Microsoft Visual Studio 2005 environment.

To adjust the measurements to a common scale and take the size of the face into consideration, the Gaussian curvature was normalized by a constant face size index, the distance between the two inner eye corners. A software Meshlab v1.2.0 (Apr 30, 2009)[78] performs the function of measuring the distance between two arbitrary points on a 3D mesh surface. The distance measurements were repeated twice at different times and then averaged. They were proceeded by a single person to ensure consistency and avoid inter-observer error.[79] Since the principal curvatures have units of inverse distance, the Gaussian curvature was normalized by multiplying the square of this normalizing factor. *S.I.* is scale invariant, and we do not need to normalize this.

The distribution of normalized Gaussian curvature *K* and the Shape Index *S.I.* were visualized by color coded maps (Figure 3.4) for the face to provide an intuitive understanding of facial geometry. In view of the fact that there was no sufficient content obtained from the patients for the use of images for publication, a model of unilateral facial paralysis simulated by a normal participant was used as the demo in this study.

By observing the color distribution of the color maps in Figure 3.4, the following Gaussian curvature and the Shape Index characteristics of the face are noted:

I. The nose tip appears as a region of high Gaussian curvature (GC > 9) and high Shape Index (S.I. > 0.90), corresponding to the geometric features of a dome or spherical cap.

II. The nasion appears as a region of low Gaussian curvature (GC < -6) and intermediate Shape Index (0.4 < S.I. < 0.6), corresponding to the geometric features of a saddle shape.

III. The region outside the features (eyes, nose, mouth) appears as regions of intermediate Gaussian curvature (-1 < GC < 1) but not convergent S.I..

Generally speaking, the Gaussian curvature emphasizes unevenness (cap, saddle, or cup), while the Shape Index emphasizes the type of the shape. However, common to both of these two attributes is the close correlation with the symmetry: a symmetric face would have symmetric color maps of Gaussian curvature and the Shape Index; an asymmetric face would

(a)

(b)

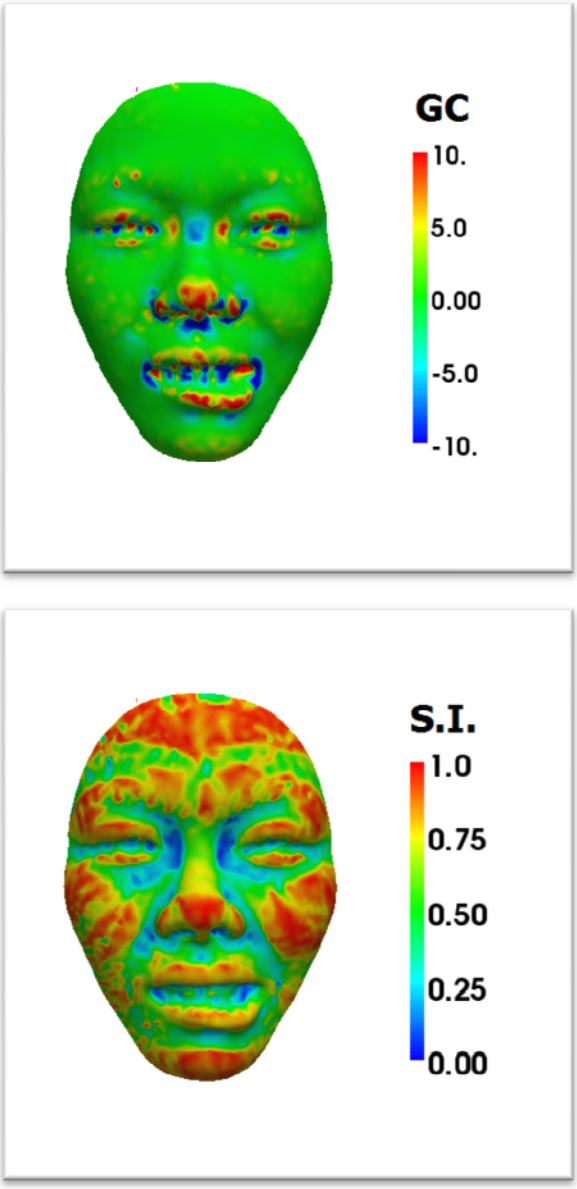

Figure 3.4 Rendering of (a) Gaussian curvature and (b) Shape Index color map on 3D face scan model of smiling to show teeth expressions.

also have asymmetric color maps of these two indices. Therefore, we may evaluate the symmetry of the face by evaluating the symmetry degree of the GC and S.I. values.

3.4 Asymmetry degree index

Since facial paralysis would cause greater asymmetric facial response of various facial motions, the extent of asymmetry, namely the asymmetry degree was evaluated and correlated with the objective grading of facial paralysis. A landmark-independent method[80,81] was adapted to determine the facial asymmetry degree by comparing the original mesh and its mirror mesh as shown in Figure 3.5. First, a mirror face mesh of the original one is generated. Then, the original mesh and its mirror one are superimposed and registered based on the Iterated Closest-Point algorithm (ICP)[82]. The algorithm iteratively applies translation and rotation on the mirror mesh to minimize the geometrical distances of two meshes. An example of the registration result is shown in Figure 3.6. The two meshes are represented in two different colors.

Based on the ICP registration result, we evaluated the asymmetry degree by measuring the matching degree between the original mesh and its mirror one. The comparison included both the geometric distance and the local contour difference described by the Gaussian curvature and the

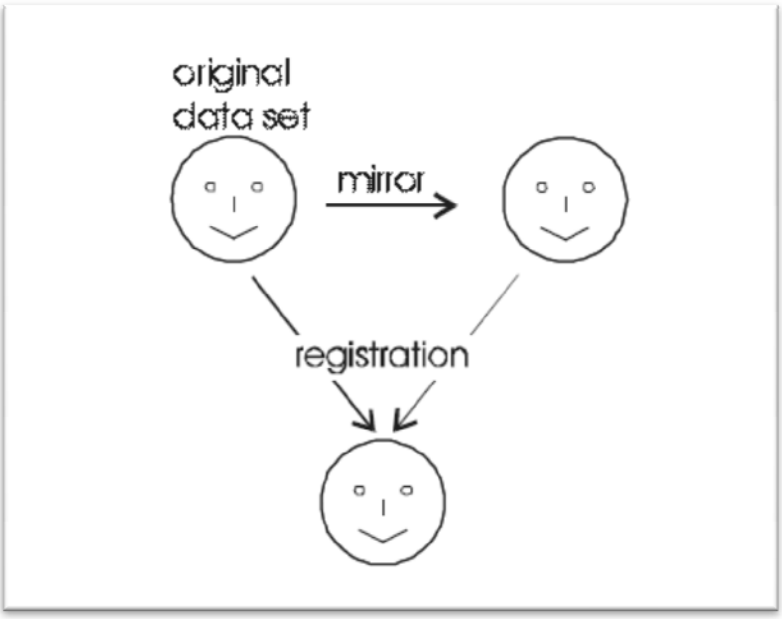

Figure 3.5 Registration between original and mirror faces by ICP.[80]

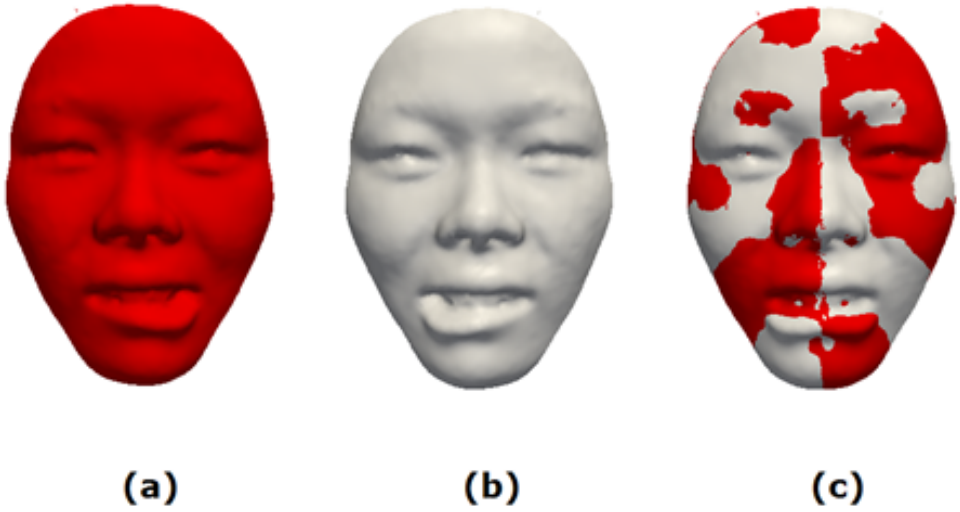

Figure 3.6 (a) Original mesh. (b) Mirror mesh. (c) ICP registration result of original and mirror meshes.

Shape Index. Before comparison, the unmatched edge of the two meshes was trimmed and excluded.

For each vertex p_i on the original mesh, we first search the nearest vertex p'_i on the mirror mesh by means of the *k-d* tree.[59] Then, the shortest distance from p_i to the vicinity triangle surface containing p'_i is calculated and assigned as the distance from p_i to the mirror mesh ($dp_i > 0$). Meanwhile, the absolute difference of the Gaussian curvature (dgc_i) and the Shape Index (dsi_i) between p_i and p'_i were also computed. As described before, normalization operation is necessary to adjust the measurements to a common scale. The distance between the two inner eye corners was used for normalization of the distance.

Figure 3.7 shows the color maps of the normalized geometric distance, the absolute difference of the Gaussian curvature, and the one of the Shape Index difference between the original and superimposed mirror meshes for one mesh sample.

(a)

(b)

(c)

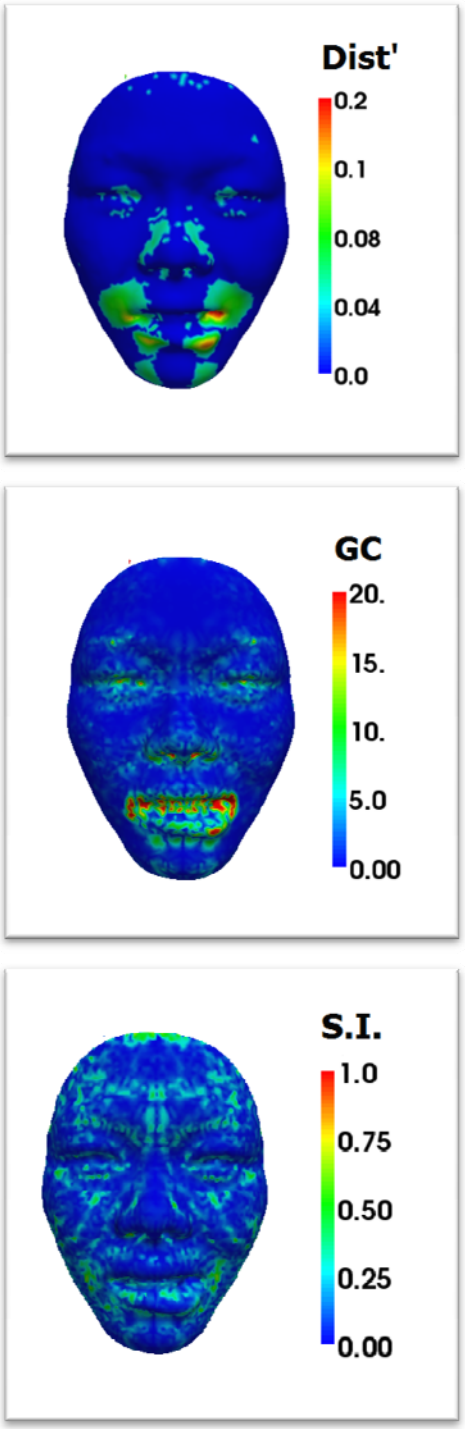

Figure 3.7 Color maps of the difference between the original and mirror meshes. (a) Geometry Distance, (b) difference of the Gaussian curvature and (c) difference of the Shape Index.

By observing the color distribution of the color maps in Figure 3.7, the threshold values of the distance, the Gaussian curvature and the Shape Index were chosen as shown in Table 3.1. The points of the original mesh with a value higher than the threshold would be considered not matched to any point on the mirror mesh. Then, the percentages of the matching points on the whole mesh for each index were calculated as asymmetry degree index for further analysis: RD for distance, RGC for the Gaussian curvature, and RSI for the Shape Index. Apparently, the values of these three indices are closely related to the degree of asymmetry of the face, and thus the severity of the disease.

Table 3.1 Threshold value chosen for no-match points filter.

Distance	Gaussian Curvature	Shape Index
0.01	**1.5**	**0.08**

3.5 Noise Injected Neural Network

Artificial neural networks (ANNs) are capable of learning from training samples presented to them and capturing the correlation between the input variables and their corresponding outputs without any prior knowledge. The excellent predictive ability of ANNs has been proven in a

wide range of issues including medical diagnosis.[83] In this study, MLP ANNs,[84,85] the most commonly used ANNs, were implemented to perform a pattern classification for facial paralysis. All data processing of neural networks was performed offline using Matlab.

Since the index RD is essentially a geometric measurement, and RGC and RSI are 3D contour measurements, we combined them to two groups as the input of the ANN classifier: {RD, RGC} and {RD, RSI}. The performance of these two input groups would be compared. For each sample subject (one person), we calculated the average index values of the four facial models separately for the three indices as the input of the neural networks. Each ANN has two input nodes corresponding to the two indices, a single hidden layer of six hidden nodes with hyperbolic tangent sigmoid transfer functions, and one binary output node with linear activation functions representing the diagnosis result.

When the training samples are rare, overfitting is common that trained ANNs could only provide the satisfied output for those well-trained inputs while their performance is poor for random samples. For regularization algorithm,[86] a popular solution for overfitting, the necessity of a separate validation set is very difficult to be satisfied by such a small

data set. To reduce the effect of overfitting caused by the use of a small training set, the noise injection method[87] was used to expand the training set. Noise injection is capable of enhancing the ANNs' generalization ability on unknown data. This method is based on the assumption that ANNs should produce similar outputs for similar inputs. Some synthetic training samples were first created by adding random noise to each of the original samples. For a training set with n training samples, p noise vectors were first generated independently all at once and injected to each input vector while keeping the output unchanged to produce new training samples. Thus, the training set was expanded to $n + np$ samples prior to training process. Then, the new training set was applied to train the networks in the conventional manner. The ratio of sample numbers of each class usually remained unchanged. In this manner, the decision boundary of the neural networks classifier would be smoother. Then, the regularization algorithm for MLP implemented by the training algorithm called "trainbr" of MATLAB neural network toolbox is applied to stop the training process before the network begin to over-fit the noise.

The noise vectors were randomly generated by zero mean Gaussian distribution functions. The variances of these noise vectors are essential to control the effects of the method. Ideal variances should properly extend

the ANN training samples to the underlying samples in the feature space. If the variances are too small, then these noises would have little effect of inhibiting overfitting during the training process. On the other hand, with too large variances of noise, the classes of the training sample set would become indistinguishable. Intuitively, addition of noise may make the classification boundary smoother. As a result, the generalization performance of the neural networks is significantly improved.[74] In our study, we applied various variance values and numbers of injected noise subjects to find out the optimal noise strength for better performance.

3.6 Performance Evaluation

As previously mentioned, we had sample sets of eight patient subjects and twelve healthy subjects. The sample set was small as it is not easy to obtain sizable human subject volunteers in a single clinic. Moreover, there were five out of eight patients who were also followed up and photographed during the clinical sessions. These samples were used to examine the sensibility of the classifier to detect the improvement of the patients' condition.

A four-fold cross validation procedure was performed in training the ANNs. All the original subjects were first divided into four subsets, each having two patient samples and three normal samples. Sequentially one subset was tested using the classifier system trained on the remaining 15 samples and the new samples generated by adding random noise on them. Thus, each subject of the whole training set was predicted once in the entire process, and the cross-validation accuracy was the percentage of the test data that were correctly classified. For the same training and test data sets, we trained each ANN 100 times with different initial weight values. In this manner, the prediction accuracy on this set could more precisely reflect the performance on classifying unknown data. The performance of the conventional ANNs and noise-injected ANNs using different training sets were compared.

3.7 Results

The goal of our work was to establish an objective facial paralysis diagnosis system having good generalization performance with a small training sample set.

To assess the performance of the ANNs, the test samples were grouped into the following four categories.[88,89]

1. True positive (TP): The ANN classifies a patient sample as a patient.

2. True negative (TN): The ANN classifies a healthy sample as a normal.

3. False positive (FP): A normal sample is labeled as a patient by the ANN.

4. False negative (FN): A patient sample is labeled as a normal by the ANN.

The performance of the neural networks was evaluated in terms of accuracy, sensitivity and specificity as follows:

Accuracy A_{cc}: The rate of the total subjects correctly classified.

$$A_{cc} = (TP + TN)/(TP + TN + FP + FN) \qquad 3.1$$

Sensitivity S_e: The rate of the patient subjects correctly detected.

$$S_e = TP/(TP + FN) \qquad 3.2$$

Specificity S_p: The rate of the normal subjects correctly detected.

$$S_p = TN/(TN + FP) \qquad 3.3$$

To investigate the performance of noise injection method, we simulated adding 60, 150, and 300 artificial subjects with different noise variance of 0.05 and 0.1 into the training set prior to training process. Classification results of the training neural networks without and with injected noise prior to conventional training are summarized in Table 3.2 for {RD, RGC} and Table 3.3 for {RD, RSI}.

It can be seen that although the original data set is rather small, the ANNs are still able to provide reasonable classifications for the samples in the test set. Compared with training the ANNs with original training set, training with noise-injected sample sets was able to overcome the problem of overfitting and significantly improve the performance of the ANNs. Basically, the performance of the ANNs with the input group of {RD, RGC} is much better than the ones with {RD, RSI}. The maximum accuracy and specificity were reached when a set of 150 noise-injected training samples were added and noise variance value of 0.05 was applied. With the same size of noised training set, and noise variance value of 0.1, the maximum sensitivity value was reached.

Table 3.2 Results provided by the ANNs with input of {RD, RGC} in the conventional manner and with noise-injected methods.

Number of training samples	Noise variance	A_{cc} (%)	S_e (%)	S_p (%)
Original 15		68.3	75.8	63.3
Noised 15 + 60	0.05	74.3	77.9	71.9
	0.1	76.6	81.5	73.3
Noised 15 + 150	0.05	78.6	84.1	74.9
	0.1	77.3	80.6	75.0
Noised 15 + 300	0.05	72.8	76.8	70.2
	0.1	70.1	74.9	66.9

Table 3.3 Results provided by the ANNs with input of {RD, RSI} in the conventional manner and with noise-injected methods.

Number of training samples	Noise variance	A_{cc} (%)	S_e (%)	S_p (%)
Original 15		61.2	68.8	56.1
Noised 15 + 60	0.05	64.8	77.0	56.7
	0.1	65.0	75.8	57.8
Noised 15 + 150	0.05	72.5	81.0	66.8
	0.1	70.8	78.3	65.8
Noised 15 + 300	0.05	69.6	77.8	60.0
	0.1	67.2	77.9	57.8

To verify the sensitivity of the proposed diagnosis system to the improvement of the patients after medical treatments, the ANN having the highest accuracy and specificity was also tested by the 3D samples of the patients taken for their follow-up visit, and compared with the diagnosis result given by clinician based on the SFGS. Totally 5 pairs of patient data were tested on the ANN having the best performance, which was trained with a set of 75 noise-injected training samples and the noise variance value of 0.05.

Table 3.4 Diagnosis results comparison for the patients before and after medical treatments

		Patient 1	**Patient 2**	**Patient 3**	**Patient 4**	**Patient 5**
Visit 1	**SFGS**	18	30	45	18	13
	ANN	*P	P	P	P	P
Visit 2	**SFGS**	63	100	67	18	91
	ANN	N	N	N	P	N
Agreement		**Y	Y	Y	Y	Y

*The diagnosis of ANN is represented by P for positive and N for negative.

** The agreement of the two diagnosis by SFGS and ANN is represented by Y for yes and N for no.

The comparison of the diagnosis results by SFGS and noise-injected ANN is shown in Table 3.4. The 100% agreement of these two diagnosis methods indicates that our proposed objective diagnosis system can well detect the improvement of the patients after medical treatments.

3.8 Discussion and Conclusion

An automated facial paralysis diagnosis system based on objective 3D image asymmetry grading is presented in this work. Different from traditional 2D image based diagnosis systems, 3D Gaussian curvatures and the Shape Index are applied to provide local contour information for 3D model analysis. To overcome the subjectivity encountered by the landmark based computer aided grading methods, we achieved facial symmetry grading based on the fine registration result of the original and mirror facial meshes by the ICP, which does not rely on any manually set landmarks. The analysis results are not sensitive to the position of the head or the size of the face. However, the face boundary could affect the classification result, and should be carefully determined in the preprocessing steps.

To avoid overfitting caused by small sample set, we applied noise injected MLP ANNs in feature extraction and classification for 3D objects. The results in Table 3.2 and Table 3.3 validate the classification system proposed in this study. Our method allows the system to improve accuracy, sensitivity as well as specificity. Overfitting was reduced by smoothening the decision boundary near the original samples with artificial samples around them. Therefore, the generalization ability of the system was increased. The number of injected noise subjects and the variance of the noises relevant influence factors of the output of the neural network. Too many noise samples and too large noise injected would reduce the accuracy of the diagnosis. Compared to the rather small size of the data set, the performance of the system was rather high. As the classifier inputs, the index group of {RD, RGC} was more effective than the group of {RD, RSI}.

We also tested the system having the highest accuracy with scan data of five patients having follow-up diagnosis after the medical treatment. These data are applied to verify the sensitivity of the classifier to the improvement of the patients. The trained noise injected MLP classifier has provided promising results with 100% agreement with the diagnosis result given by clinicians to the follow-up cases. The MLP system can well detect the improvement of the patients. A plausible explanation of the appreciably improved performance is that the injected noise increases the generalization ability, and reduces the

sensitivity to the disturbance in this way. Noise injected neural network should be considered as effective diagnosis tools, especially when the clinic dataset is small. Meanwhile, the proposed system would demonstrate a more adequate performance if it is trained with larger sample dataset.

In summary, we verified that the proposed 3D image based noise injected ANN system was a suitable tool for facial paralysis diagnosis. Gaussian curvatures applied in this study provided useful local contour information for classification. The performance of our ANN classifier was trained and tested on a data set with the total of 20 subjects. An accuracy of 78.6% and a sensitivity of 84.1% were achieved by the developed MLP ANN with a relative small data set. Therefore, the proposed system could be useful for facial paralysis diagnosis.

Chapter 4. Facial Highlight Features Analysis

4.1 Introduction

Analyzing the highlight features is complex work. Because of the central position of nose, it is usually considered to be the most prominent feature. Based on interviews with practicing plastic surgeons, we start our analysis from nose, and then extend to the whole face (Figure 4.1). This study will quantitatively compare facial features across race and gender.

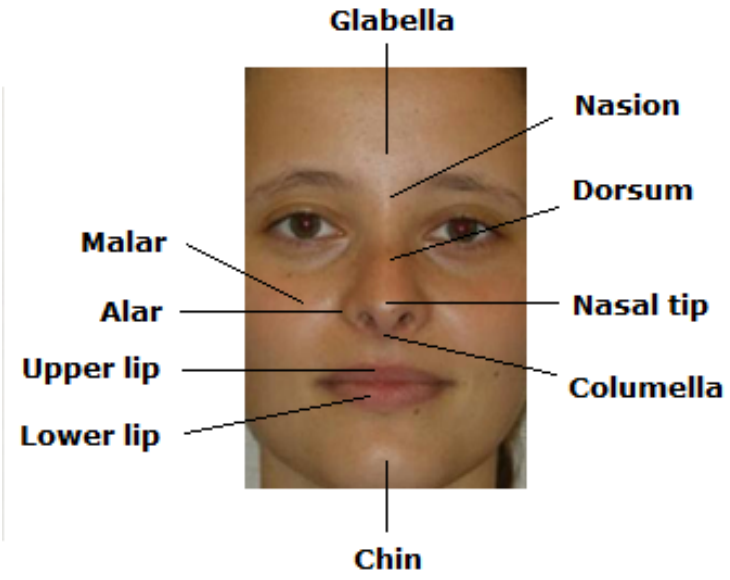

Figure 4.1 Anatomy of human face.

More specifically, this study seeks to address the following questions, which were brought up by clinicians of plastic surgery:

1) Identify the positions and basic schemas of the highlight regions. Till now, the location and shape of this highlight region has yet to be studied.

2) Study the schema of forehead highlight region.

3) Determine the shape of the nasion according to race and gender by the survey of the Gaussian curvature.

4.2 Data Acquisition

In this research, we employed a database of randomly selected 64 human subjects consisting of 37 Chinese (18 males, 19 females), 19 Eurasians (8 males, 11 females) and 8 Caucasians (6 males, 2 females), aged between 16-40 years. The Chinese subjects trace their origins from Southern China, the Caucasian subjects from the European continent, and the Eurasian subjects have a heritage including ancestors of both Caucasian and Chinese origins. The subjects were evenly divided by gender, and none of these subjects had taken any facial cosmetic surgery. For details of age, race and gender on the subjects, please see Table 4.1.

Approval from the relevant Institutional Review Board (IRB) had been obtained prior to the study.

Table 4.1 Age, race and gender information of sample subjects

		Age 16~30	Age above 30
Chinese	**Male**	**14**	**5**
	Female	**13**	**5**
Eurasian	**Male**	**2**	**6**
	Female	**5**	**6**
Caucasian	**Male**	**5**	**1**
	Female	**2**	**0**

2D colorful facial images with neutral face expression of the subjects have been used extensively in the extraction of facial highlights. Both anterior and lateral views of the faces were captured in a reproducible and controlled illuminating environment. Figure 4.2 shows the images taken for six subjects of different race and gender.

(a)

(b)

(c)

(1) **(2)**

Figure 4.2 Anterior and lateral facial views of six sample subjects. Rows correspond to six subjects of (a) Chinese male, (b) Chinese female, (c) Eurasian male, (d) Eurasian female, (e) Caucasian male, and (f) Caucasian female. Columns correspond to different views of (1) anterior view, and (2) lateral view.

Meanwhile, the 3D data of these faces had also been collected by using plaster casts of nose region of all the subjects, and the casts were subsequently captured in 3D using a 3dMD system. The 3D face models were stored in the form of triangulated meshes.

(a)

(b)

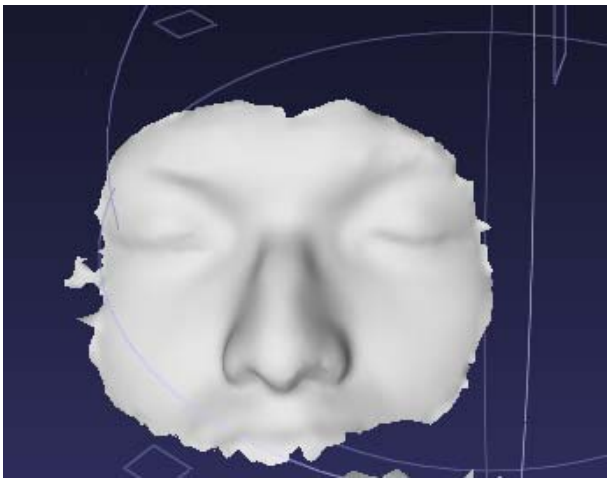

Figure 4.3 (a) Plaster cast of nose region; (b) 3D model reconstructed by scanning the plaster cast.

4.3 Highlight region extraction

The Adobe Photoshop CS3 software was applied to extract the highlight region on the images. We demonstrate this process with Figure 4.3 (a.1), first.

Figure 4.4 Grayscale image with nose tip landmark *prn* and alar landmark *al* added.

The first step was to convert the original color image of anterior face to grayscale image (Figure 4.4). The gray levels in the images are integers in the range of [0, 255]. Second, in order to extract the highlight regions, a threshold of gray level was set and the gray image was converted to black and white mode. The threshold value should be between the gray level of the brightest highlight point and the dark area. Based on our observation, the brightest highlight point is at the nasal tip *prn*, and the edge of nasal alar *al* is the dark point. So we set the gray

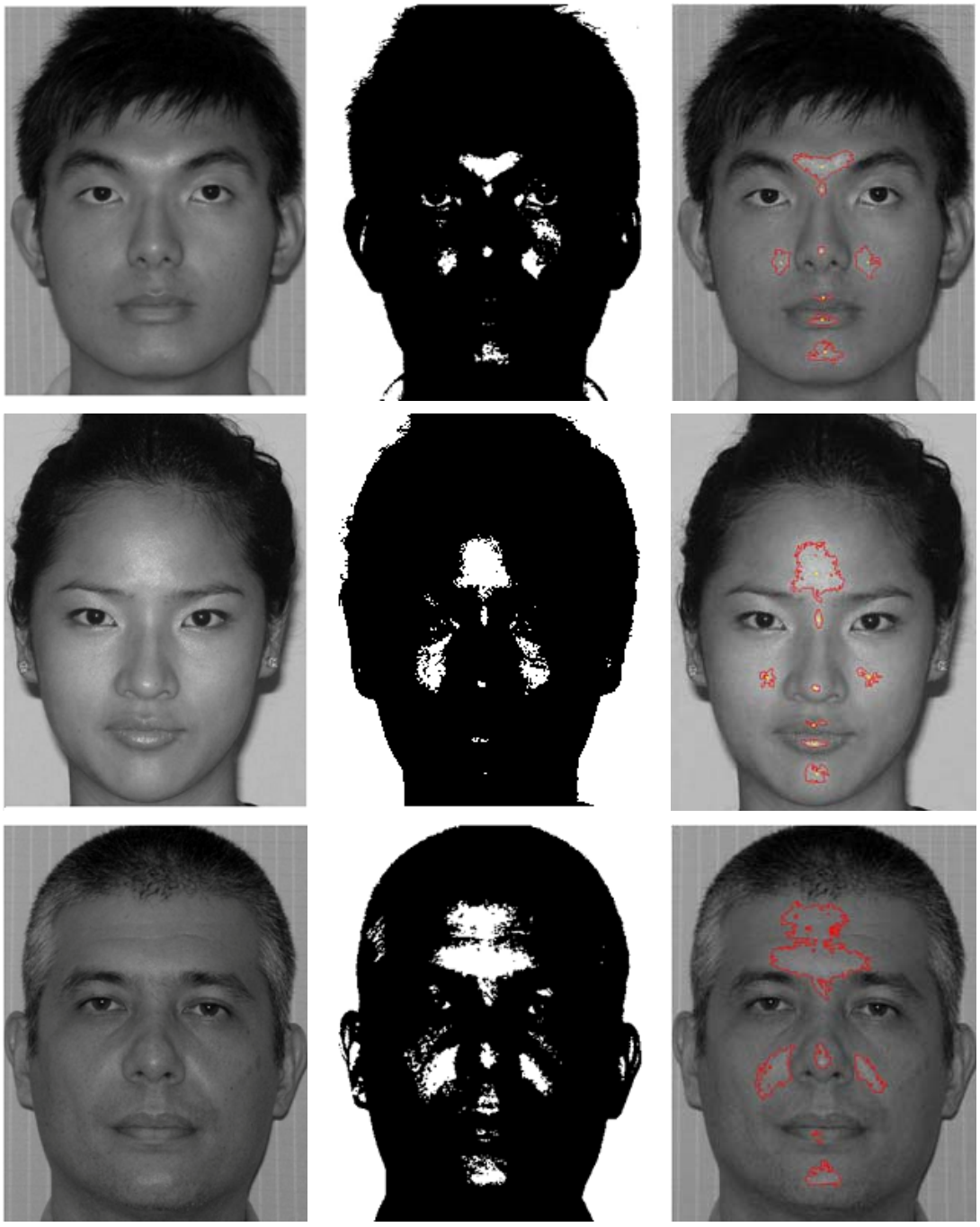

(a)

(b)

(c)

(1) **(2)** **(3)**

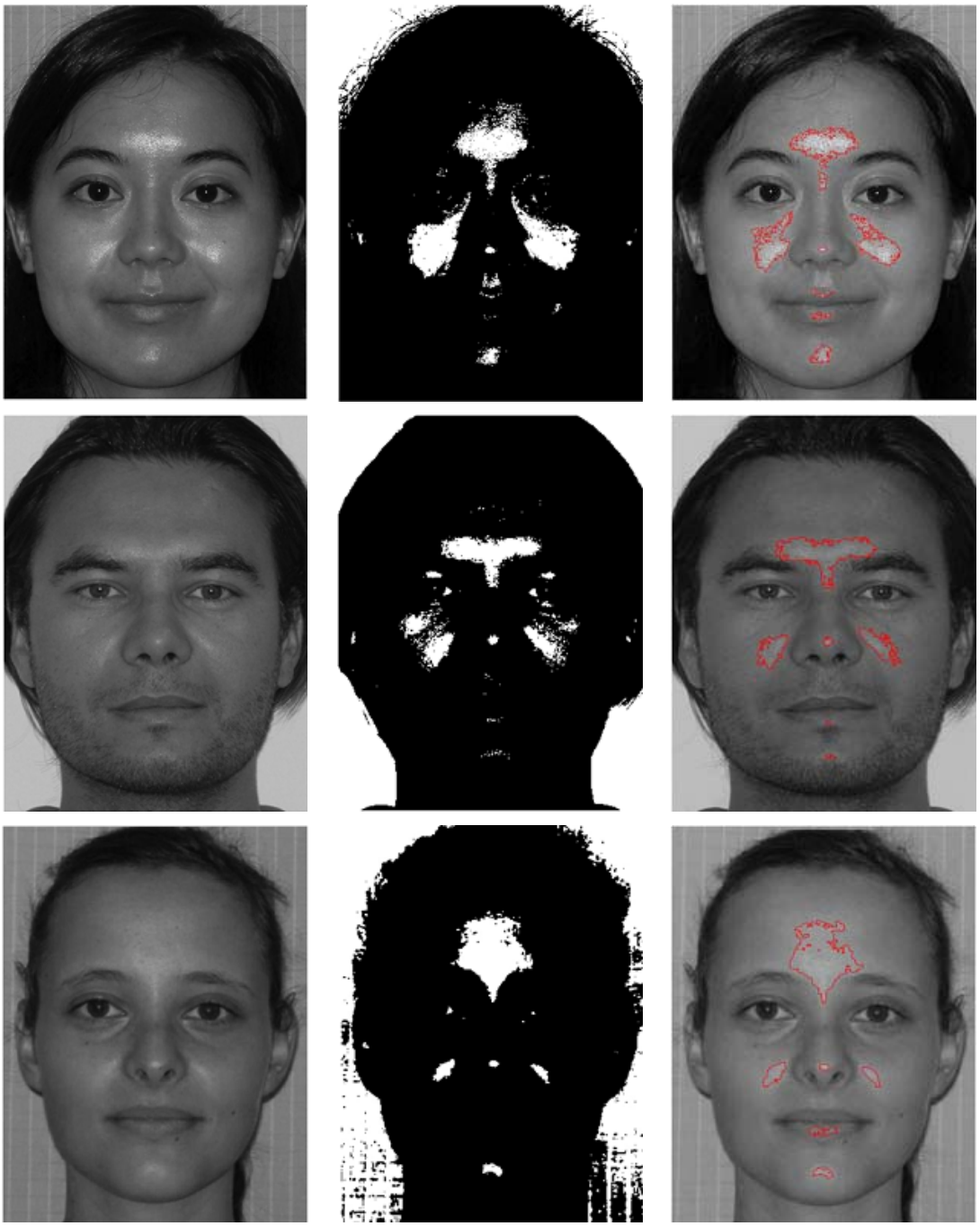

Figure 4.5 Facial highlight region extraction process. Rows correspond to six subjects of (a) Chinese male, (b) Chinese female, (c) Eurasian male, (d) Eurasian female, (e) Caucasian male, and (f) Caucasian female. Columns correspond to highlight extraction steps of (1) grayscale image, (2) setting gray level threshold for grayscale image, and (3) extracted highlight regions.

level threshold value as the mean value of the gray level of *prn* and the one of *al*. Then the grayscale image was transferred to a black and white mode image, and the white areas on the face are the extracted highlight regions. The corresponding regions were separated on the grayscale image for further analysis. The white regions corresponding to the white eyes were ignored since they are not the highlight regions. We did this highlight extraction process to all of the 64 subjects. Figure 4.5 shows the highlight extraction process results of the previous six sample subjects.

4.4 Facial highlight features

In this section, we will discuss some schemas of the facial highlight regions. Thereafter, Fisher's exact test was applied to examine the correlations among the race and gender factors.[90,91]

Fisher's exact test is a statistical test used to compare proportions between independent groups and examine the significance of the association between the two kinds of classification when the outcome variables are binary or categorical (e.g. gender, yes/no). Different from other tests with similar functions, it is valid when there are sparse data (some cells <5).

4.4.1 Highlight regions distribution

As we can see from Figure 4.5, there are actually six consistent regions of highlight: forehead (glabella and nasion), two malar projection, nasal tip, central lower lip, and chin projection. Some samples also have highlight region on upper lip. Some samples have separated glabella and nasion highlights.

4.4.2 Highlight of nasal bridge

Although modern makeup artists generally make a continue highlight along the nasal bridge, by checking the results of the 64 subjects, we did not find a subject with a continue highlight from the nasion down to the nasal tip. For the most cases, there is one highlight at the forehead, and one spot at the nasal tip. Only a few cases have a bar highlight along the nasal bridge, but broken between the nasion and the nasal tip. For the nasal bridge highlight details of race and gender on the subjects, please see Table 4.2. This indicates that on natural face, the highlights of the bridge are broken in half rather than appear in whole. This may explain why many nasal implants may make the nose looks fake if they are straight all the way down the nose. Creating a perfectly straight highlight on the nasal bridge appears unnatural.

Table 4.2 Race and gender distributions of the highlight shape on the nasal bridge.

	Missing	Bar highlight	Amount
Chinese			
Total	**30 (81.1%)**	**7 (18.9%)**	**37**
Male	**13 (72.2%)**	**5 (27.8%)**	**18**
Female	**17 (89.5%)**	**2 (10.5%)**	**19**
Eurasian			
Total	**18 (94.7%)**	**1 (5.3%)**	**19**
Male	**8 (100%)**	**0 (0%)**	**8**
Female	**10 (90.9%)**	**1 (9.1%)**	**11**
Caucasian			
Total	**6 (75%)**	**2 (25%)**	**8**
Male	**4 (66.7%)**	**2 (33.3%)**	**6**
Female	**2 (100%)**	**0 (0%)**	**2**

4.4.3 Schema of forehead highlight region.

Basically, all the forehead highlight regions can be divided into two types. For the first type, the shape of the highlight region is like the one in Figure 4.6 (a), which resembles the capital letter T. It is usually located in the middle of the two eyebrows. We named it as T shape. For the second type, the shape of the region is more like an upside-down maple leaf as shown in Figure 4.6 (b), and we named this as maple leaf shape. The position of the center is higher than the one of T shape.

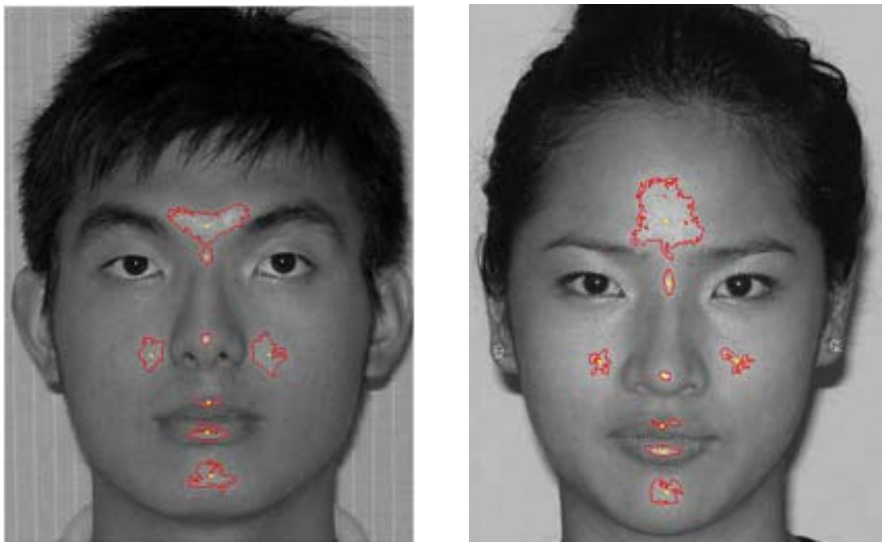

(a) **(b)**

Figure 4.6 Two type of forehead highlight regions: (a) T shape, and (b) Maple leaf shape.

To investigate the correlations of both race and gender along with the forehead highlight shape, the subjects were categorized and counted according to race, gender, and shape. Then, Fisher's exact test was applied to examine the correlations among these factors.

This study included 64 randomly chosen Chinese, Eurasian, and Caucasian subjects who had never undergone any facial cosmetic surgery. The forehead highlight regions of these subjects were extracted from their anterior images. Table 4.3 shows the number of subjects per forehead highlight type along with race and gender distributions.

Table 4.3 Race and gender distributions of the forehead highlight shape for the 64 subjects.

	T shape	Maple leaf shape	Amount
Chinese			
Total	**24 (65%)**	**13 (35%)**	**37**
Male	**17 (94.4%)**	**1 (5.6%)**	**18**
Female	**7 (36.8%)**	**12 (63.2%)**	**19**
Eurasian			
Total	**8 (42.1%)**	**11 (57.9%)**	**19**
Male	**3 (37.5%)**	**5 (62.5%)**	**8**
Female	**5 (45.5%)**	**6 (54.5%)**	**11**
Caucasian			
Total	**1 (12.5%)**	**7 (87.5%)**	**8**
Male	**1 (16.7%)**	**5 (83.3%)**	**6**
Female	**0 (0%)**	**2 (100%)**	**2**

The distinct forehead highlight region shape proportion differences were observed between the race and gender groups. For Chinese subjects, the percentage of maple leaf shape subjects is only 35%, whereas for the Caucasian population, this value is as high as 87.5%. It shows that maple leaf shape is much more common for Caucasian people, while T shape is more common for Chinese people. Eurasian people fall between the other two populations. By using Fisher's exact test on the statistical data according to race only, significant correlation of race and forehead highlight shape was confirmed ($p = 0.017$).

For Chinese subjects, we found that the proportion of T shape highlight of the male group is much higher than the one of the female group. With a rather small p value of 0.00036, the Fisher's exact test proved that Chinese men and women have huge different forehead highlight shape aspect. However, there were no significant differences found between the two gender subgroups for Eurasian and Caucasian groups.

As such, the above statistical results suggest that the forehead highlight region shape is quite related to race and gender.

The shape and position of the facial highlights have been considered as important aspects when performing various types of plastic surgeries. The desired highlight shape and position tell us where exactly to put in the fillers or implants to create a healthy, natural, and attractive face.

After extracting forehead highlight from the anterior image for all the subjects, we found out two shape schemas of this region, T shape and maple leaf shape. Referring to the lateral images of these subjects, the ones with T shape highlight usually have lower and more flat forehead and higher superciliary arches. On the contrary, the ones with maple leaf shape highlight usually have a higher forehead, and a less prominent superciliary arch.

Meanwhile, the statistical data show that there is large shape proportion difference among the three race groups. The proportion of maple leaf in the Chinese group is the lowest, while the one in the Caucasian group is the highest. These facts should be determined by different gene structure. Since Eurasians are the mixed ancestry of Chinese and Caucasians, it is not difficult to understand that the statistical values of the Eurasian group are all between the corresponding ones of the Chinese and Caucasian groups. However, the reason why there is significant shape proportion difference between the two genders of Chinese subjects is still unknown.

4.5 3D Objective Measurement of the surface contour

The reconstructed 3D models of the subjects allowed us to calculate the Gaussian curvature. The program was developed using Visual C++ under Microsoft Visual Studio 2005 environment. The two-way ANOVA is used to test for differences according to race and gender. If the null hypothesis of the ANOVA F-test is rejected ($p < 0.05$), a statistical difference exists between the population means. In that case, the Tukey's HSD test is carried out to make a pair-wise comparison between each population mean to determine if there is a statistical difference.

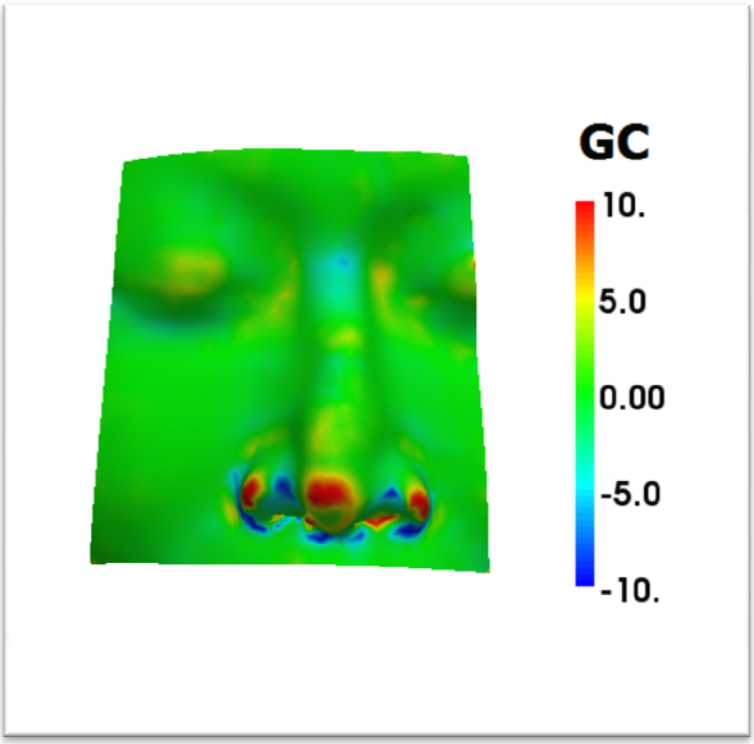

Figure 4.7 Gaussian curvature value color map

The statistical analysis works were achieved by the software R[92], an SPSS-like statistical analysis tool which conducts analyses such as ANOVA (Analysis of Variance), the Tukey's HSD (Honestly Significant Difference) test, as well as the Fisher's test.

We surveyed the lowest Gaussian curvature value of the nasion region for each sample and analyzed the correlation between this index along with race and gender. A two-way ANOVA analysis was used to test the differences according to race and gender. It was determined that gender was not a significant factor. However, Gaussian curvature at the nasion differed significantly across race, F

(2, 63) = 3.342, p = 3.5E-05. Tukey's HSD comparisons of the three levels of race indicate that Eurasians (Mean = 0.0905) have a significantly lower Gaussian curvature at the nasion than Chinese (Mean = 0.0623), Caucasians (Mean = 0.0953) have a significantly lower Gaussian curvature at the nasion than Chinese. Comparisons between Eurasians and Caucasians were not significantly different (p = 0.912).

We also tested the relationship between the Gaussian curvature and the forehead highlight shape using ANOVA test. The result showed that the Gaussian curvature at the nasion differed significantly across the forehead highlight shape, F (1, 62) = 3.918, p = 5.63E-03. Tukey's HSD comparisons of the two forehead highlight shape indicate that the subjects of maple leave shape (Mean = 0.580) have a significantly lower Gaussian curvature at the nasion than the ones of T shape (Mean = 0.548).

Chapter 5. Conclusion

There are mainly two parts in this study. First, we developed a novel automated objective asymmetry grading system for facial paralysis diagnosis. The development of this grading system combined observations and clinical assessments of the patients for different degrees of motion dysfunction in various facial expressions. To improve the performance of the system, we involved higher order surface properties in facial imaging technique for 3D model analysis. 3D principle curvatures, Gaussian curvatures and S.I. were essentially considered. Also, to overcome the subjectivity encountered by the landmark based computer aided grading methods, we achieved facial symmetry grading based on fine registration result of the original and mirror facial mesh by the ICP algorithm, which does not rely on any landmarks. Moreover, to avoiding overfitting caused by small sample set, we applied noise injected ANNs in feature extraction and classification for 3D objects.

Compared with standard MLP ANNs, accuracy and specificity of our proposed noise-injected ANNs are significantly better, while sensitivity remains the same. We also tested the system with data of six patients

having follow-up diagnosis after recovery. These data are applied to verify the sensitivity of the classifier to the improvement of the patients. The trained noise injected ANNs classifier was capable of identifying 100% of the recovered patient samples as normal cases. The ANNs system can well detect the improvement of the patients. A plausible explanation of the appreciably improved performance is that the injected noise increases the generalization ability, and reduces the sensitivity to the disturbance in this way.

Different from most of the reported works, this study provides a novel landmark-independent method for evaluating the degree of facial paralysis. Based on higher order surface measurements, the Gaussian curvature and the Shape Index, which describe local contour of the surface rather than simply provide the position, the novel method improves performance compared to previous 3D based works.

Due to our method which is based on facial asymmetry grading, we only considered unilateral facial dysfunction caused by Bell's palsy. The other very few conditions were not included in our research. However, Bell's palsy covers all of the conditions except for cases caused by brain tumor, stroke, and Lyme disease, which is the most common condition of facial

paralysis. Also, only rare cases (1%), facial paralysis occurs bilaterally resulting in total facial paralysis (Bell's palsy information site). Hence, we were capable of covering the majority of all cases in practice.

There are some meaningful directions for future work in the area of computer aided facial paralysis grading research.

As we know, facial paralysis causes patients loss partial facial expression functions. This is also the reason why clinical diagnosis of this disease is made mainly based on facial presentation of several different expressions. However, the importance of these expressions could be quite different, which has not been well studied. Rough set theory specializes in knowledge reduction in decision table, and is well suitable for the assessment for the attributes significance, which represent the importance of different expressions in this case.

Although noise-injected method has improved the performance of our classification system, we still believe in that the small data size limits the study. The MLP ANNs would be more reliable if it is trained by larger data set. In practice, the intensity difference of people's facial expression was noticed. Some patients are used to have less facial expression. They are hard to be diagnosed correctly by the classifier trained by data of usual

people. Also, the current clinical judgments of each patient sample were from only one professional assessor. The diagnosis data from multiple assessors would be more reliable and objective.

For the facial highlight study, the highlight feature patterns of natural faces are analyzed based on interviews with practicing plastic surgeons. Since data is still missing on where these highlights should be on natural faces, especially on faces of different ethnic descent and gender, this study intends to determine the position and shape of the highlights of natural faces across race and gender. Such knowledge may assist cosmetic surgeon in planning aid for plastic surgery. Some relevant conclusions can be drawn from the present study. First, there are mainly six consistent regions of highlight: forehead, two malar projection, nasal tip, central lower lip, and chin projection. Second, we found out that nasal highlights are discontinuous. Only a few cases have a bar highlight along the nasal bridge, but broken between the nasion and the nasal tip. For the most cases, there is one highlight at the forehead, and one spot at the nasal tip. Also, the forehead highlight has mainly two types, T shape and maple leaf shape. The distributions of these two types are closely related to race and gender. Furthermore, by surveying the Gaussian curvature, we found out that the shape of the nasion saddle is intimately associated with race.

References

1. Bowyer KW. Face recognition technology: security versus privacy. Technology and Society Magazine, IEEE 2004; 23:9-19.

2. BBC. Japanese smokers to face age test. Available at: http://news.bbc.co.uk/2/hi/asia-pacific/7395910.stm.

3. Lin C. Face detection in complicated backgrounds and different illumination conditions by using YCbCr color space and neural network. Pattern Recognition Letters 2007; 28:2190-2200.

4. Whitehill J, Littlewort G, Fasel I, Bartlett M, Movellan J. Toward practical smile detection. Pattern Analysis and Machine Intelligence, IEEE Transactions on 2009; 31:2106-2111.

5. Kanerva M. Peripheral facial palsy: Grading, Etiology, and Melkersson-Rosenthal Syndrome 2008.

6. Peitersen E. Bell's palsy: the spontaneous course of 2,500 peripheral facial nerve palsies of different etiologies. Acta Oto-Laryngologica 2002; 122:4-30.

7. Skorin L. Bell's palsy: Diagnosis and management. Available at: http://www.optometry.co.uk/clinical/details?aid=360.

8. Kevin Tsai: I can still host the Golden Horse Awards. Available at: http://entertainment.xin.msn.com/en/celebrity/buzz/asia/kevin-tsai-i-can-still-host-the-golden-horse-awards.

9. Tiemstra JD, Khatkhate N. Bell's palsy: diagnosis and management. Am Fam Physician 2007; 76:997-1002.

10. Furuta Y, Ohtani F, Kawabata H, Fukuda S, Bergström T. High prevalence of varicella-zoster virus reactivation in herpes simplex virus-seronegative patients with acute peripheral facial palsy. Clinical infectious diseases 2000; 30:529-533.

11. House JW, Brackmann DE. Facial nerve grading system. Otolaryngology--head and neck surgery: official journal of American Academy of Otolaryngology-Head and Neck Surgery 1985; 93:146.

12. House JW. Facial nerve grading systems. The Laryngoscope 1983; 93:1056-1069.

13. Brackmann D, Barrs D. Assessing recovery of facial function following acoustic neuroma surgery. Otolaryngology--head and neck surgery: official journal of American Academy of Otolaryngology-Head and Neck Surgery 1984; 92:88.

14. Kahn J, Gliklich R, Boyev K, Stewart M, Metson R, McKenna M. Validation of a patient-graded instrument for facial nerve paralysis: the FaCE scale. The Laryngoscope 2001; 111:387.

15. Linstrom CJ. Objective facial motion analysis in patients with facial nerve dysfunction. The Laryngoscope 2002; 112:1129-1147.

16. Beurskens CHG, Heymans PG. Positive effects of mime therapy on sequelae of facial paralysis: stiffness, lip mobility, and social and physical aspects of facial disability. Otology & Neurotology 2003; 24:677-681.

17. Coulson SE, Croxson GR, Adams RD, O'Dwyer NJ. Reliability of the "Sydney," "Sunnybrook," and "House Brackmann" facial grading systems to assess voluntary movement and synkinesis after facial nerve paralysis. Otolaryngol Head and Neck Surgery 2005; 132:543-549.

18. Neely J, Joaquin A, Kohn L, Cheung J. Quantitative assessment of the variation within grades of facial paralysis. The Laryngoscope 1996; 106:438.

19. May M. Facial paralysis, peripheral type: a proposed method of reporting.(Emphasis on diagnosis and prognosis, as well as electrical and chorda tympani nerve testing). The Laryngoscope 1970; 80:331-390.

20. Stennert E. Facial nerve paralysis scoring system *Facial Nerve Surgery, Proceedings: Third International Symposium on Facial Nerve Surgery, Zurich*, 1976:543-547.

21. K. A, A. M, J.M. Tet al. Classification and standardized documentation of surgical results *Proceedings of the Third International Symposium on Facial Nerve Surgery*. Zurich, Switzerland: Aesculapius Publishing, 1977:527-554.

22. Fisch U, Pillsbury HC. Infratemporal fossa approach to lesions in the temporal bone and base of the skull. Archives of otolaryngology (Chicago, Ill: 1960) 1979; 105:99.

23. Fisch U. Surgery for Bell's palsy. Archives of otolaryngology (Chicago, Ill: 1960) 1981; 107:1.

24. S.E. C, G. C. Assessing physiotherapy rehabilitation outcomes following facial nerve paralysis. Australian Journal of Otolaryngology 1995; 2:20-24.

25. Smith I, Murray J, Cull R, Slattery J. Facial weakness: a comparison of clinical and photographic methods of observation. Archives of Otolaryngology—Head & Neck Surgery 1991; 117:906-909.

26. Smith I, Murray J, Cull R, Slattery J. A comparison of facial grading systems. Clinical Otolaryngology & Allied Sciences 1992; 17:303-307.

27. Ross BG, Fradet G, Nedzelski JM. Development of a sensitive clinical facial grading system. Otolaryngology--Head and Neck Surgery 1996; 114:380-386.

28. Adour K, Swanson Jr P. Facial paralysis in 403 consecutive patients: emphasis on treatment response in patients with Bell's palsy. Transactions-American Academy of Ophthalmology and Otolaryngology American Academy of Ophthalmology and Otolaryngology 1971; 75:1284.

29. Kayhan FT, Zurakowski D, Rauch SD. Toronto facial grading system: interobserver reliability. Otolaryngology--Head and Neck Surgery 2000; 122:212-215.

30. Isono M, Murata K, Tanaka H, Kawamoto M, Azuma H. An objective evaluation method for facial mimic motion. Otolaryngology--Head and Neck Surgery 1996; 114:27-31.

31. Scriba H, Stoeckli S, Pollak A, Veraguth D, Fisch U. Objective evaluation of normal facial function. The Annals of otology, rhinology & laryngology 1999; 108:641-644.

32. Dulguerov P, Marchal F, Wang D, Gysin C. Review of objective topographic facial nerve evaluation methods. Otology & Neurotology 1999; 20:672-678.

33. Chatrath P, De Cordova J, Nouraei SAR, Ahmed J, Saleh HA. Objective assessment of facial asymmetry in rhinoplasty patients. Archives of Facial Plastic Surgery 2007; 9:184-187.

34. Wachtman G, Liu Y, Zhao Tet al. Measurement of asymmetry in persons with facial paralysis *Proceedings of Combined Annual Conference of the Robert H. Ivy and Ohio Valley Societies of Plastic and Reconstructive Surgeons*, 2002.

35. McGrenary S, O'Reilly BF, Soraghan JJ. Objective grading of facial paralysis using artificial intelligence analysis of video data *Computer-Based Medical Systems, 2005. Proceedings. 18th IEEE Symposium on*: IEEE, 2005:587-592.

36. Wang S, Li H, Qi F, Zhao Y. Objective facial paralysis grading based on Pface and eigenflow. Medical and Biological Engineering and Computing 2004; 42:598-603.

37. He S, Soraghan JJ, O'Reilly BF. Biomedical Image Sequence Analysis with Application to Automatic Quantitative Assessment of Facial Paralysis. EURASIP Journal on Image and Video Processing 2007; 2007:1-11.

38. Thompson DW. On growth and form. On growth and form 1942.

39. Andie Macdowell Plastic Surgery Before & After Photos. Available at: http://plasticsurgeryc.com/andie-macdowell-plastic-surgery-before-after-photos/.

40. Park S. Facial plastic surgery: the essential guide. Thieme, 2005.

41. Vinci Ld. Vitruvian Man: Leonardodavinci.stanford.edu, 1490.

42. Farkas L. Anthropometry of the head and face. 1994: Raven Press, New York.

43. Jefferson Y. Facial beauty - establishing a universal standard. INTERNATIONAL JOURNAL OF ORTHODONTICS-MILWAUKEE-2004; 15:9-26.

44. Gunes H, Piccardi M. Assessing facial beauty through proportion analysis by image processing and supervised learning. International Journal of Human-Computer Studies 2006; 64:1184-1199.

45. Woodard CR, Park SS. Nasal and facial analysis. Clinics in plastic surgery 2010; 37:181-189.

46. Jones R. Makeup Makeovers: Expert Secrets for Stunning Transformations. Beauty Bible. Fair Winds, 2011.

47. Wang C, Principe JC. Training neural networks with additive noise in the desired signal. Neural Networks, IEEE Transactions on 1999; 10:1511-1517.

48. Brown WM, Gedeon TD, Groves DI. Use of noise to augment training data: a neural network method of mineral–potential mapping in regions of

limited known deposit examples. Natural Resources Research 2003; 12:141-152.

49. Moreno AB, Sánchez A, Vélez JF, Díaz FJ. Face recognition using 3D surface-extracted descriptors *Irish Machine Vision and Image Processing Conference*: Citeseer, 2003.

50. Colombo A, Cusano C, Schettini R. 3D face detection using curvature analysis. Pattern recognition 2006; 39:444-455.

51. Gaba E. View of the planes establishing the main curvatures on a minimal surface. Wikipedia, 2006.

52. Koenderink JJ, van Doorn AJ. Surface shape and curvature scales. Image and vision computing 1992; 10:557-564.

53. Dorai C, Jain AK. COSMOS-A representation scheme for 3D free-form objects. Pattern Analysis and Machine Intelligence, IEEE Transactions on 1997; 19:1115-1130.

54. Zhong L, Su Y, Yeo SY, Tan RS, Ghista DN, Kassab G. Left ventricular regional wall curvedness and wall stress in patients with ischemic dilated cardiomyopathy. American Journal of Physiology-Heart and Circulatory Physiology 2009; 296:H573-H584.

55. Yeo SY, Zhong L, Su Y, Tan RS, Ghista DN. A curvature-based approach for left ventricular shape analysis from cardiac magnetic resonance imaging. Medical & biological engineering & computing 2009; 47:313-322.

56. NN C. Differential geometry for surveying engineers. University of New Brunswick, Frederiction, 1985.

57. Willmore TJ. An introduction to differential geometry. DoverPublications. com, 2012.

58. Besl PJ, McKay ND. Method for registration of 3-D shapes *Robotics-DL tentative*: International Society for Optics and Photonics, 1992:586-606.

59. Zhang Z. Iterative point matching for registration of free-form curves and surfaces. International journal of computer vision 1994; 13:119-152.

60. Pulli K. Multiview registration for large data sets *3-D Digital Imaging and Modeling, 1999. Proceedings. Second International Conference on*: IEEE, 1999:160-168.

61. Rusinkiewicz S, Levoy M. Efficient variants of the ICP algorithm *3-D Digital Imaging and Modeling, 2001. Proceedings. Third International Conference on*: IEEE, 2001:145-152.

62. Hecht-Nielsen R. On the algebraic structure of feedforward network weight spaces. Advanced Neural Computers 1990:129-135.

63. Zurada JM. Introduction to artificial neural systems 1992.

64. Fausett L. Fundamental of neural networks. Florida Institute of Technology 1994; 4.

65. Parten C, Hartson C, Maren A, Pap R. Handbook of neural computing applications 1990.

66. Aizenberg I. Complex-valued neural networks with multi-valued neurons. Springer, 2011.

67. Shahin MA, Jaksa MB, Maier HR. Artificial neural network applications in geotechnical engineering. Australian Geomechanics 2001; 36:49-62.

68. Moselhi O, Hegazy T, Fazio P. Potential applications of neural networks in construction. Canadian Journal of Civil Engineering 1992; 19:521-529.

69. Flood I, Kartam N. Neural networks in civil engineering. I: Principles and understanding. Journal of Computing in Civil Engineering 1994; 8:131-148.

70. Maier HR, Dandy GC. Neural networks for the prediction and forecasting of water resources variables: a review of modelling issues and applications. Environmental modelling & software 2000; 15:101-124.

71. Gardner M, Dorling S. Artificial neural networks (the multilayer perceptron)--a review of applications in the atmospheric sciences. Atmospheric environment 1998; 32:2627-2636.

72. Liu Y, Starzyk JA, Zhu Z. Optimized approximation algorithm in neural networks without overfitting. Neural Networks, IEEE Transactions on 2008; 19:983-995.

73. Ding S, Xiang C. Overfitting problem: a new perspective from the geometrical interpretation of MLP *Design and application of hybrid intelligent systems*: IOS Press, 2003:50-57.

74. An G. The effects of adding noise during backpropagation training on a generalization performance. Neural Comput 1996; 8:643-674.

75. Wikipedia. Bell's palsy. Available at: http://en.wikipedia.org/wiki/Bell%27s_palsy#References.

76. Kau CH, Richmond S. The three dimensional surface acquisition system for facial analysis. Three dimensional imaging for orthodontics and maxillofacial surgery Kau CH, Richmond S 2010; 1:11-28.

77. Kanerva M, Poussa T, Pitkäranta A. Sunnybrook and House-Brackmann Facial Grading Systems: intrarater repeatability and interrater agreement. Otolaryngology-Head and Neck Surgery 2006; 135:865-871.

78. Cignoni P Version 1.2.0. Visual computing lab - ISTI - CNR; 2009.

79. Farkas LG. Accuracy of anthropometric measurements: past, present, and future. The Cleft palate-craniofacial journal 1996; 33:10-22.

80. M. B, X. L, T. Met al. The Symmetry of Faces *Vision, Modeling, and Visualization. Amsterdam: IOS Press*, 2002:332-339.

81. Hartmann J, Meyer-Marcotty P, Benz M, Häusler G, Stellzig-Eisenhauer A. Reliability of a method for computing facial symmetry plane and degree of asymmetry based on 3D-data. Journal of Orofacial Orthopedics/Fortschritte der Kieferorthopädie 2007; 68:477-490.

82. Laboureux X, Häusler G. Localization and registration of three-dimensional objects in space-where are the limits? Applied optics 2001; 40:5206-5216.

83. Forsström JJ, Dalton KJ. Artificial neural networks for decision support in clinical medicine. Annals of medicine 1995; 27:509-517.

84. Haikin S. Neural networks: a comprehensive foundation. Prentice Hall, 1998.

85. Howard D, Beale M. Neural Network Toolbox, for Use with MATLAB, User's Guide, Version 4, The MathWorks. Inc product 2000:133-205.

86. Sarle WS. Stopped training and other remedies for overfitting *Proceedings of the 27th Symposium on the Interface* 1995:352-360.

87. Matsuoka K. Noise injection into inputs in back-propagation learning. Systems, Man and Cybernetics, IEEE Transactions on 1992; 22:436-440.

88. Tarassenko L, Khan YU, Holt MRG. Identification of inter-ictal spikes in the EEG using neural network analysis. Science, Measurement and Technology, IEE Proceedings - 1998; 145:270-278.

89. Özbay Y. A New Method for Diagnosis of Cirrhosis Disease: Complex-valued Artificial Neural Network. Journal of Medical Systems 2008; 32:369-377.

90. Fisher RA. On the interpretation of χ 2 from contingency tables, and the calculation of P. Journal of the Royal Statistical Society 1922; 85:87-94.

91. Agresti A. A survey of exact inference for contingency tables. Statistical Science 1992:131-153.

92. Ripley BD. The R project in statistical computing. MSOR Connections 2001; 1:23-25.